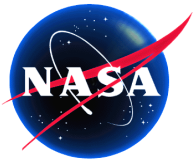

Ion Propulsion System (NSTAR) DS1 Technology Validation Report

John R. Brophy, Roy Y. Kakuda, James E. Polk, John R. Anderson, Michael G. Marcucci, David Brinza, Michael D. Henry, Kenneth K. Fujii, Kamesh R. Mantha, John F. Stocky
Jet Propulsion Laboratory
California Institute of Technology
Pasadena, California 91109

James Sovey, Mike Patterson, Vince Rawlin, John Hamley
Glenn Research Center
Cleveland, Ohio

Tom Bond, Jon Christensen, Hap Cardwell, Gerald Benson, Joe Gallagher
Hughes Electron Dynamics Division
Torrance, California

Mike Matranga
Spectrum Astro, Inc.
Gilbert, Arizona

Duff Bushway
Moog, Inc.
Aurora, New York 13026

JPL

Table of Contents

Section Page

Figures

Figure Page

Tables

Page

Appendices

Appendix

EXTENDED ABSTRACT

1.0 TECHNOLOGY VALIDATED

The *Deep Space 1* (DS1) spacecraft uses a single-engine, xenon ion propulsion system, provided by the NASA Solar electric propulsion Technology Applications Readiness (NSTAR) project, for primary on-board propulsion.

Technology-validation requirements for the NSTAR Project were developed early in the project life cycle. A quality functional deployment (QFD) exercise conducted in 1993 resulted in a documented set of user, customer, stakeholder, and sponsor needs that the NSTAR Project needed to satisfy in order to be declared successful. All items from that complete list are shown in this report along with the benchmark data that was demonstrated in flight. One of the prime objectives of the project was to satisfy future users that this technology was flight-proven; therefore, retiring the perceived risk issues was a significant part of the validation effort. The details of these efforts are described in the full report. Some of these important issues were retired through an extensive ground test program while the others were retired through the flight test on DS1.

2.0 RISKS ASSOCIATED WITH THIS TECHNOLOGY

The following key risks were addressed by the NSTAR project as part of ground testing and during the flight of the ion propulsion system on DS1:

1. Adequate engine life—Prior to the NSTAR project, no ion engine intended for primary propulsion had ever been successfully operated for its full design life.
2. Guidance, navigation and control (GN&C) of a solar-electric propulsion (SEP) spacecraft—The low-thrust nature of SEP, together with large solar arrays, makes GN&C sufficiently different from conventional deep-space spacecraft that this is a significant risk area.
3. Mission operation costs—SEP systems require the propulsion system to operate continuously for long periods of time, leading some observers to project that a standing army of propulsion and power engineers would be required to operate the spacecraft, resulting in high-mission operations costs.
4. Spacecraft contamination by the SEP system—Slow erosion of the engine results in a non-propellant efflux from the thruster that could contaminate sensitive spacecraft surfaces.
5. SEP impacts on science instruments—The charge-exchange plasma generated by the operation of the SEP system is easily detected by on-board plasma instruments.
6. SEP impacts on communication—The charge-exchange plasma generated by the operation of the SEP system, as well as the primary beam plasma, could affect the transmission or reception of electromagnetic waves.
7. Electromagnetic compatibility (EMC) of the SEP system with the spacecraft—The high-power nature of SEP and the use of strong permanent magnets in the ion engines could make it difficult for the SEP system to be electromagnetically compatible with the spacecraft.

How these risks were successfully retired is discussed in the full report.

3.0 VALIDATION OBJECTIVES AND APPROACH

The NSTAR project was designed to overcome the barriers preventing the use of SEP on deep-space missions and enable ion propulsion to enter the mainstream of deep-space propulsion options. To accomplish this, the project had to achieve two major objectives:

1. Demonstrate that the NASA 30-cm diameter ion engine had sufficient life and total impulse capability to perform missions of near-term interest.
2. Demonstrate through a flight test that the ion propulsion system hardware and software could be flight qualified and successfully operated in space and that control and navigation of an SEP-based spacecraft could be achieved.

To demonstrate sufficient engine life, the ground test program was designed to first demonstrate 100% of the engine design life and, subsequently, to demonstrate 150% of the engine life. The flight of the NSTAR system on DS1 addressed the integration, compatibility, and operations issues associated with the use of SEP on a deep space mission.

4.0 TEST PROGRAM

The NSTAR test program employed an extensive ground test activity together with the flight test on DS1 to validate the ion propulsion technology.

The NSTAR ground test program was planned around the use of engineering model thrusters (EMTs) built by NASA Glenn Research Center (GRC) and eventually flight model thrusters fabricated by Hughes Electron Dynamics (HED). A total of four EMTs and two sets of flight hardware—consisting of thrusters, power processor units (PPUs), and digital interface & control units (DCIUs)—were fabricated and tested. In addition, the NSTAR project designed and fabricated an engineering model xenon feed system. The flight xenon control assembly (XCA) was fabricated by Moog. The four EMTs enabled a series of more than 40 engineering tests that addressed wear mechanisms, thermal behavior, mechanical fidelity, low-power performance, and, finally, lifetime in order to instill confidence in the thruster design. An 8000-hour life test demonstrated—for the first

time in history—that an ion engine for primary propulsion could be successfully operated for its full design life.

The two sets of flight units were subjected to acceptance and qualification testing, after which selected flight units were delivered to the spacecraft for the DS1 test program and, ultimately, for flight. The spare flight set is, as of this writing, being used in an extended life test to demonstrate 150% of the engine design life.

5.0 TEST RESULTS

Ground Tests

Early tests of the GRC-built engineering model thrusters validated an initial set of design features and enabled measurement of engine-component wear under a variety of thruster operating conditions. A 2000-hour test of EMT1 led to design improvements that were successfully verified in a subsequent 1000-hour test of this thruster. These tests resulted in a final design that was incorporated into the second engineering model thruster, EMT2. This thruster was used in the Life Demonstration Test (LDT), which was designed to operate the thruster for 8000 hours at full power.

The LDT was the most successful endurance test of a high-power ion engine ever performed. A total of 8,192 hours of operation were achieved at an input power of 2.3 kW with a specific impulse of 3200 s before it was voluntarily terminated. A total of 88 kg of xenon propellant was processed, demonstrating a total impulse of 2.73×10^6 N-s. Risks associated with neutralizer lifetime, thrust performance degradation, engine efficiency degradation, material deposition, thrust vector drift, electrode wear, long-term thermal characteristics, and initial start-up conditions were successfully retired by this test.

The last major test in the NSTAR project plan is the Extended Life Test (ELT), which is designed to demonstrate 150% of the engine design life using the DS1 flight spare engine (FT2). The engine design life is most easily expressed in terms of the total amount of xenon propellant that the thruster can process. For the NSTAR project, the engine design life is 82 kg of xenon, which corresponds to about 8,000 hours of operation at full power. To demonstrate 150% of the engine life, therefore, requires a test in which approximately 125 kg of xenon is processed by the engine. A secondary objective of this test is to demonstrate extended operation at throttled conditions since the previous project-level life tests had all been performed at the full-power point. It is believed that the full-power point is the most stressing to the engine; however, the ELT is designed to obtain the data necessary to support this assertion.

As of this symposium (February 2000), the ELT has operated FT2 for more than 8,000 hours covering three different throttle levels and has processed more than 75 kg of xenon. The test is scheduled to demonstrate the 125-kg throughput by the end of the year. The Deep Space Exploration Technology program is considering extending this test to determine the actual thruster end-of-life. This would significantly benefit the potential future users listed in Section 6.0 below.

Flight Test

Aside from an initial hiccup, the operation of the NSTAR ion propulsion system (IPS) on DS1 has been flawless.

The initial hiccup occurred 4.5 minutes after the engine was first started in space when continuous high-voltage recycling caused the thruster to shutdown. Subsequent troubleshooting efforts identified that the fault was most likely due to a piece of conductive debris lodged between the grids. To dislodge this debris, the spacecraft was turned several times to move the ion engine in and out of the Sun. This results in thermally cycling of the engine's ion accelerator system causing the electrodes to move relative to one another. Subsequently, another start attempt was made at thirty-one days after launch. The engine started normally and has operated perfectly since this time.

As expected, operation of the ion engine, PPU, and xenon feed system in space produced performance that closely matched that measured on the ground. In addition, the flight on DS1 enabled the following resolution of the key risk areas listed earlier:

1. Guidance, navigation and control—The operation of the SEP system on DS1 demonstrated that GN&C is not more difficult with an SEP spacecraft, just different.
2. Mission operation costs—The electrical nature of SEP lends itself well to autonomous operation, resulting in essentially no significant increase in mission operations cost for SEP vehicles.
3. Spacecraft contamination—Data from DS1 indicates that this efflux travels largely in line-of-sight from the engine and does not pose a significant health risk to a properly designed spacecraft.
4. SEP impact on science instruments—DS1 showed that the low-energy, charge-exchange plasma generated by the operation of the ion engine does not interfere with measurements of the much more energetic solar wind plasma
5. SEP impacts on communication—No impact of the SEP system operation on communications with DS1 could be detected.
6. Electromagnetic compatibility (EMC) of the SEP system with the spacecraft—DS1 showed that while this issue requires careful engineering, it is an easily tractable problem.

6.0 Applicability and Potential Future Benefits

Many missions have been identified by JPL's advanced mission planning activity as being either enabled or strongly enhanced by the use of solar electric propulsion. These were based on NSTAR or derivatives of the NSTAR ion propulsion technology, including: Comet Nucleus Sample Return, Mercury Orbiter, Neptune Orbiter, Titan Explorer, Saturn Ring Observer, Europa Lander, and Venus Sample Return.

To illustrate the benefits enabled by the use of an NSTAR-derivative SEP system for a mission to a comet, the performce of a SEP-based spacecraft to the comet 46P/Wirtanen is compared to ESA's chemical propulsion-based Rosetta mission to the same target. The Rosetta spacecraft has an initial wet mass of 2,900 kg and is launched on an Ariane 5. This spacecraft takes more than 9 years to reach the comet, arrives with a net spacecraft mass of 1300 kg, and does not return a sample from the comet. An SEP-based spacecraft, on the other hand, with an initial wet mass of 1830 kg, could be launched on a Delta IV medium launch vehicle. The SEP system would take only 2.6 years to deliver a 1300-kg spacecraft to the comet. The same SEP system could then return the spacecraft and a comet sample to Earth in an additional 4.5 years. Thus, the SEP-based spacecraft could travel to the comet and return to Earth in less time than it takes for a chemical-propulsion-based spacecraft to fly to the comet!

7.0 Conclusions

The success of the NSTAR SEP system on the DS1 spacecraft, as well as the success of the NSTAR engine life test program, has resulted in SEP now becoming a legitimate propulsion option for deep space missions. The project's successful validation effort now enables exciting new missions to benefit from the substantial performance capabilities of ion propulsion.

NSTAR Fact Sheet

GRC GLENN RESEARCH CENTER at Lewis Field — JPL

The NSTAR project and DS1 successfully validated ion propulsion enabling exciting new missions to benefit from the substantial performance capabilities of this technology

Flight Engine Performance Measured in Space

NSTAR Throttle Level	Mission Throttle Level	PPU Input Power (kW)	Engine Input Power (kW)	Measured Thrust (mN)	Main Flow Rate (sccm)	Cathode Flow Rate (sccm)	Neutralizer Flow Rate (sccm)	Specific Impulse (s)	Total Efficiency
12	85	1.99	1.86	75.34	19.99	2.91	2.82	3035	0.602
11	83	1.94	1.82	72.55	18.63	2.75	2.67	3125	0.610
11	83	1.96	1.83	72.63	18.62	2.75	2.67	3131	0.609
10	77	1.84	1.72	69.54	18.59	2.75	2.67	3000	0.594
10	76	1.82	1.70	67.21	17.31	2.58	2.51	3109	0.602
10	75	1.79	1.68	66.81	17.33	2.58	2.51	3087	0.601
10	74	1.77	1.66	66.11	17.33	2.59	2.51	3054	0.595
10	73	1.75	1.65	65.64	17.31	2.59	2.51	3035	0.594
10	72	1.73	1.63	65.15	17.31	2.59	2.51	3012	0.592
9	69	1.67	1.57	62.27	16.08	2.50	2.43	3070	0.597
6	48	1.29	1.22	47.43	11.42	2.50	2.42	3006	0.573
6	48	1.29	1.22	47.39	11.44	2.49	2.42	3004	0.571
3	27	0.89	0.84	31.70	6.93	2.50	2.43	2770	0.511
0	6	0.50	0.48	20.77	6.05	2.50	2.43	1961	0.418

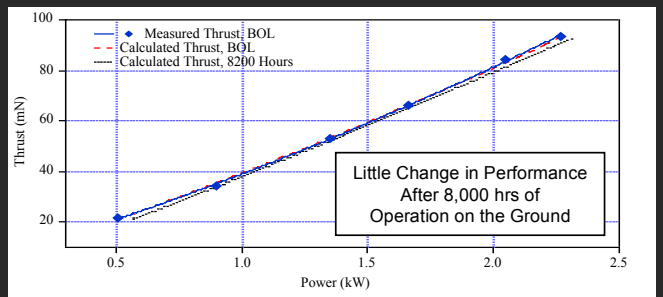

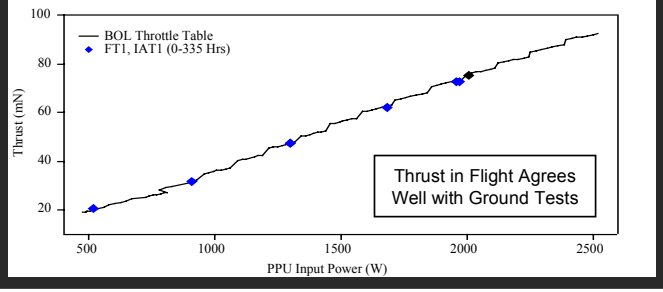

JPL 2/00

Thruster

Thrust	19.0 to 92.7 mN
Input Power	423 to 2288 W
Isp	1814 to 3127 s
Mass	8.33 kg
Xe Throughput Demonstrated	88 kg
Xe Throughput Planned	125 kg by the end of Y2K
Manufacturer	Hughes Electron Dynamics

Power Processing Unit (PPU)

Input Power	474 to 2522 W
Efficiency	0.92 to 0.94
Input Voltage	80 to 160 VDC
Mass	13.3 kg
Manufacturer	Hughes Electron Dynamics

Digital Interface & Control Unit (DCIU)

S/C Interface	1553
PPU Interface	RS-422
Mass	2.47 kg
Manufacturer	Spectrum Astro, Inc.

Xenon Feed System

Flow Rate Accuracy	+/-3%
Cathode, Neutralizer Flow	2.39 to 3.7 sccm
Main Flow	5.98 to 23.43 sccm
Xenon Control Assembly (XCA)	7.78 kg
XCA Manufacturer	Moog, Inc.
Plenum Tanks (two)	1.5 kg (each)
Tank Assembly Mass	7.94 kg
Tank Volume	49.2 liters
Mass of Xenon Stored	81.5 kg
Main Tank Manufacturer	Lincoln Composites

Ion Propulsion System (NSTAR) DS1 Technology Validation Report

John R. Brophy, Roy Y. Kakuda, James E. Polk, John R. Anderson, Michael G. Marcucci, David E. Brinza, Michael D. Henry, Kenneth K. Fujii, Kamesh R. Mantha, John F. Stocky
Jet Propulsion Laboratory, California Institute of Technology, Pasadena, California

James Sovey, Mike Patterson, Vince Rawlin, John Hamley
Glenn Research Center, Cleveland, Ohio

Tom Bond, Jon Christensen, Hap Cardwell, Gerald Benson, Joe Gallagher
Hughes Electron Dynamics Division, Torrance, California

Mike Matranga
Spectrum Astro, Inc., Gilbert, Arizona

Duff Bushway
Moog, Inc., Aurora, New York

1.0 Introduction

The first use of solar-electric propulsion (SEP) on a deep-space mission began with the launch of the Deep Space 1 (DS1) spacecraft on October 28, 1998. This marks a milestone in the development of advanced propulsion for deep-space missions. The DS1 spacecraft uses a single xenon-ion engine, provided by the NASA Solar electric propulsion Technology Applications Readiness (NSTAR) project, as the primary onboard propulsion system. This propulsion system is designed to deliver a total ΔV of 4.5 km/s to DS1 while using only 81 kg of xenon.

The NSTAR project was designed to overcome the barriers preventing the use of SEP on deep-space missions and enable ion propulsion to enter the mainstream of deep-space propulsion options. To accomplish this, the project had to achieve two major objectives:

1. Demonstrate that the NASA 30-cm diameter ion engine has sufficient life and total-impulse capability to perform missions of near-term interest.
2. Demonstrate through a flight test that the ion-propulsion system hardware and software could be flight qualified and successfully operated in space and that control and navigation of an SEP-based spacecraft could be achieved.

By all measures, these objectives have been met with unqualified success. Aside from an initial hiccup, the operation of the NSTAR ion propulsion system (IPS) on DS1 has been flawless: the IPS successfully provided the ΔV required for the July 29, 1999 flyby of the asteroid Braille. Consequently, ion propulsion is now a credible propulsion option for future deep-space missions. Details of how the NSTAR ion-propulsion technology was validated for deep-space missions are given in the sections that follow. This report is a summary version of the full NSTAR Flight Validation Report given in Reference [1].

2.0 Technical Description

As is rigorously explained in Reference [30], the NSTAR IPS was one of 12 breakthrough technologies to be validated on the DS1 spacecraft. Each was to be validated in different ways depending on the technology usage and would require different periods of time. Through joint planning, the DS1 operators and NSTAR personnel produced a validation plan that fit into the DS1 overall-mission plan. How DS1 was conceived and how the individual validation results were perceived from an overall-spacecraft perspective are also explained in Reference [30]. This paper, therefore, concentrates on the validation results from the technology's standpoint and illustrates some risk-reduction issues that could be applied to future programs.

The NSTAR project developed and delivered an ion propulsion system to DS1 that was based on the NASA 30-cm diameter xenon ion engine. This section provides a description of the NSTAR IPS, the key technology objectives, and a summary of the ground- and flight-test results.

2.1 The NSTAR Ion-Propulsion System

A block diagram of the four major components of the NSTAR IPS is given in Figure 1. The ion thruster uses xenon propellant delivered by the xenon feed system (XFS) and is powered by the power processing unit (PPU), which converts power from the solar array to the currents and voltages required by the engine. The XFS and PPU are controlled by the digital control and interface unit (DCIU), which accepts and executes high-level commands from the spacecraft computer and provides propulsion subsystem telemetry to the spacecraft-data system. To accommodate variations in the solar array output power with distance from the Sun, the NSTAR IPS was designed to operate over an engine-power range of 500 W to 2,300 W. Discrete levels within this range are often referred to as "throttle levels." The mass of the NSTAR IPS is given in Table 1.

Table 1. NSTAR IPS Component Masses

Component	Mass (kg)
Ion Engine	8.33
Power Processing Unit (PPU)	15.03
XFS minus Xenon Propellant Tank	12.81
Xenon Propellant Tank	7.66
Digital Control and Interface Unit (DCIU)	2.47
PPU to Ion Engine Cable	1.70
Total	48.00

2.1.1 Ion Engine—The NSTAR−ion engine produces thrust by ionizing a low-pressure xenon gas (of order ~ 0.1 Pa) and electrostatically accelerating the resulting positive ions. Ion acceleration is accomplished through the use of two closely spaced, multi-aperture electrodes positioned at one end of the engine across which an accelerating voltage of 1.28 kV is applied. The velocity of the ion exhaust is determined by the magnitude of the applied-net-accelerating voltage and the charge-to-mass ratio of the ions. A magnetic field created by rings of permanent magnets is used to improve the efficiency with which the engine ionizes the propellant. Electrons stripped from the propellant atoms in the ionization process are collected and injected into the positive-ion beam by the neutralizer cathode in order to space-charge neutralize the ion beam and to prevent the spacecraft from accumulating a large negative charge.

The electrostatic-acceleration process is extremely efficient. In practice, the NSTAR ion-accelerator system has an efficiency of converting electrical-potential energy to kinetic energy of ≥99.6%. This nearly perfect ion acceleration efficiency enables the ion engine to produce a specific impulse of more than 3,000 seconds while maintaining low-engine-component temperatures. It also results in the ion engine being the most efficient type of electric thruster at specific impulses greater than approximately 2,500 seconds. The combination of high efficiency and high specific impulse makes ion engines attractive for a wide variety of mission applications, including north-south station keeping (NSSK) of satellites in geosynchronous orbit, Earth-orbit transfer, orbit repositioning of Earth-viewing spacecraft, and robotic solar-system exploration.

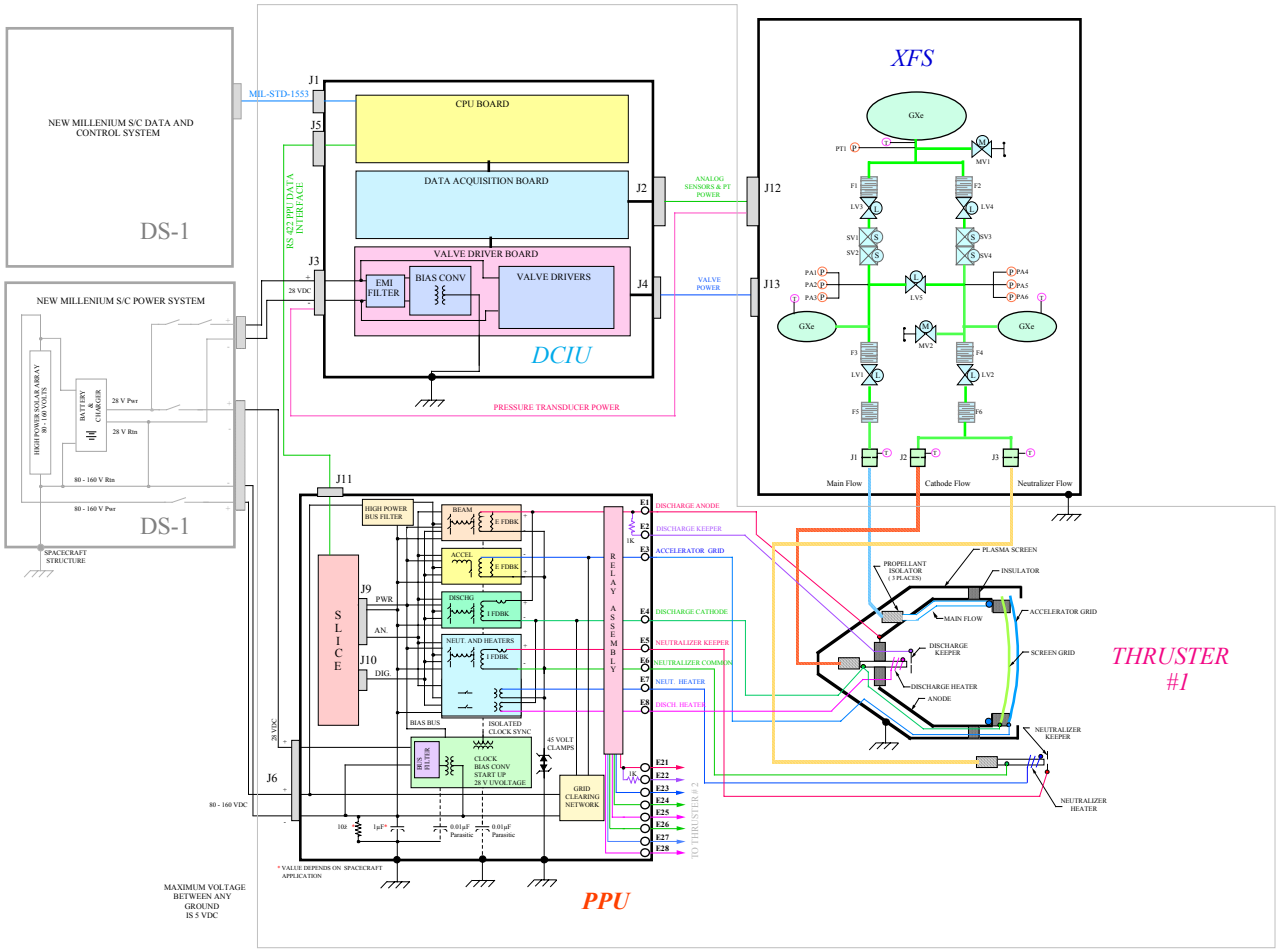

Figure 1. Functional Block Diagram of the NSTAR Ion Propulsion System

A schematic diagram of the NSTAR 30-cm diameter ion engine fabricated by Hughes Electron Dynamics (HED) is shown in Figure 2. The engine is based on technologies developed by NASA [2] and is designed to produce a thrust of 20 mN to 92 mN with a specific impulse of 1950 seconds to 3100 seconds over the input-power range of 500 W to 2,300 W. The engine-design life is 8,000 hours at the full-power-operating point. This is equivalent to a total propellant throughput capability of 83 kg and a total impulse of 2.65×10^6 N-s. The engine is designed to provide this throughput for any throttling profile.

On DS1, in order to maintain the thrust centerline through the spacecraft center of gravity (CG), the thruster is mounted on a 2-axis gimbal ring whose orientation is controlled onboard.

2.1.2 Xenon Feed System (XFS)—The NSTAR xenon-feed system, shown schematically in Figure 1, is designed to store up to 81.5 kg of xenon propellant and provide three separate flow rates to the engine: main flow, cathode flow, and the neutralizer flow. The XFS controls these flow rates to within ±3% over a range of 6 to 24 sccm for the main flow, and 2.4 to 3.7 sccm for the cathode and neutralizer flows. The flow-rate control and accuracy are achieved by controlling the pressure in the two plenum tanks upstream of the three porous-metal-plug flow-control devices (FCDs) labeled J1, J2 and J3 in Figure 1. The pressures in the plena are measured with multiple redundant pressure transducers and controlled with two bang-bang solenoid-valve regulators. The main flow is fed from one plenum, while the cathode and neutralizer-flow lines are manifolded into the other. The FCDs for the cathode and neutralizer are closely matched, so these flows are approximately equal over the entire throttling range of the engine. The flow rate through each FCD is a function of the upstream pressure and temperature; therefore, each plenum pressure is controlled by commands from the DCIU, which compensates for changes in FCD temperature to achieve the desired-flow rate. Upstream-latch valves serve to isolate the main tank from the rest of the system during launch, while the downstream-latch valves start and stop the flow to the engine during operations.

All of the XFS components except the tanks were assembled into a xenon control assembly (XCA) and mounted on a single plate by Moog, Inc. The FCD assemblies were manufactured by Mott, Inc., and the plenum tanks were manufactured by Structural Composites, Inc. (SCI). The propellant feed lines exit the XCA, cross the gimbal mechanism and attach to the engine with resistoflex fittings. The mass of the XFS given in Table 1 includes the flow-control components, the tubing, the wiring, and the XCA plate.

The xenon is stored in a super-critical state to minimize the storage volume. To maintain a single-phase state throughout the entire mission, it is necessary to maintain a minimum propellant-tank temperature of 20° C. Depending on the propellant load, if the temperature goes below this minimum, the xenon could go into a liquid state that may result in tank slosh or the injection of liquid into the feed system resulting in xenon-flow spikes. To keep the composite xenon-propellant tank from over pressurizing, the maximum temperature limit is set to 50° C. The XFS propellant tank has a volume of 49.2 liters and was manufactured by Lincoln Composites.

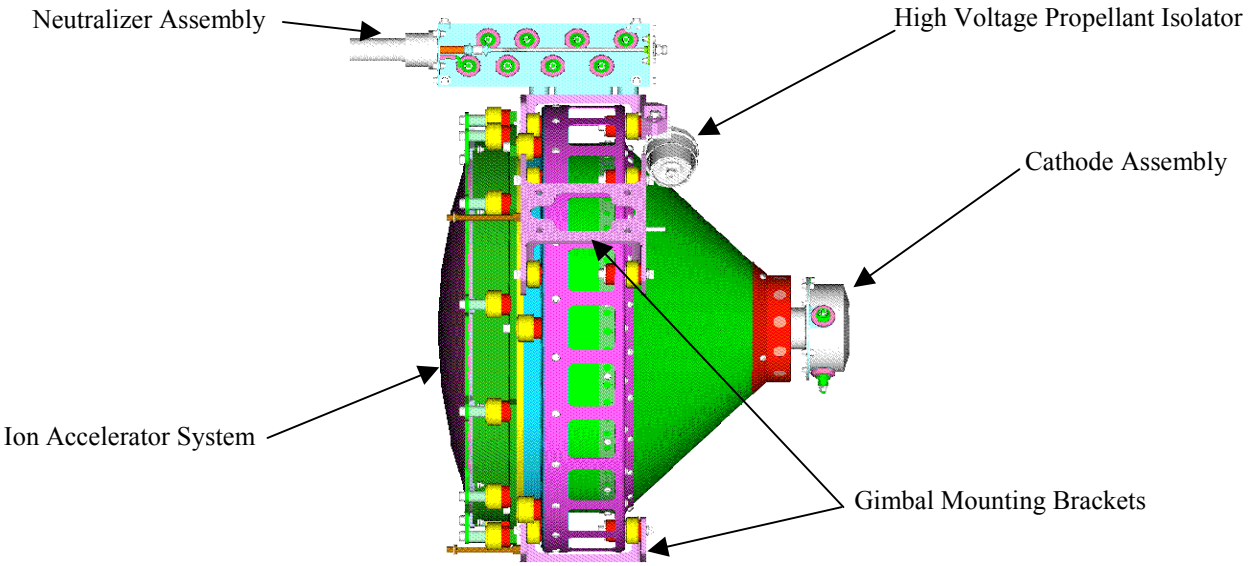

Figure 2. Diagram of the NSTAR Ion Engine (with the plasma screen removed)

2.1.3 Power Processing Unit (PPU)—The PPU is designed to take an 80 V to 160 V input directly from the solar array and supply the appropriate currents and voltages to start and operate the engine. This large input-voltage range was designed to accommodate the expected variation in solar-array-output voltage resulting from a large variation in spacecraft-Sun distance. The PPU is packaged in an enclosure separate from the DCIU and is designed to be bolted onto the spacecraft bus in an area where its excess heat output can be thermally radiated to space. In addition to the high-voltage input, the PPU requires a 28-VDC input for housekeeping power. Both input-power buses have electromagnetic-interference filters to meet the conducted emission requirements of MIL-STD-461. Enclosed within the PPU is a digital "slice" board that operates an RS422 serial-command and telemetry interface with the DCIU, digitizes the PPU telemetry, and controls the PPU-power supplies based on commands from the DCIU.

During normal-engine operation, the PPU provides four steady-state outputs. The beam voltage, the accelerator-grid voltage, the discharge current, and the neutralizer-keeper current are provided by four power supplies as shown in Figure 3. They are the beam supply, the accelerator supply, the discharge supply, and the neutralizer supply, respectively. In addition, during engine startup the PPU provides heater power to the cathode and neutralizer heaters and an ignition voltage of 650 V to the cathode and neutralizer-keeper electrodes. The PPU output requirements are summarized in Table 2. The high-voltage input to the PPU is distributed to three inverters operating at 20 kHz that drive these power supplies. The power-supply outputs are routed to internal relays thta allow them to be switched to one of two terminal blocks, so that a single PPU could be used to run either of two engines. External power-output cables attached to these terminal blocks route power to the field joint on the DS1 spacecraft.

The PPU contains internal protection for input over- and under-voltage conditions. In addition, each power supply is short-circuited protected. When a short-circuit is detected on the beam or accelerator power supplies, internal logic initiates a recycle event to clear this short, based on the assumption that this short is the result of an arc discharge between the electrodes of the ion-accelerator system. The recycle sequence includes turning both supplies off, ramping the discharge current to 4.0 A, enabling both supplies again, and then ramping the discharge current back to the original setpoint. The PPU also contains a "grid-clearing-circuit," which can be used to attempt to clear an electrical short-circuit between the accelerator-system electrodes that cannot be cleared by the recycle sequence. This circuit includes relays that place the discharge-power supply across the accelerator-system electrodes. The

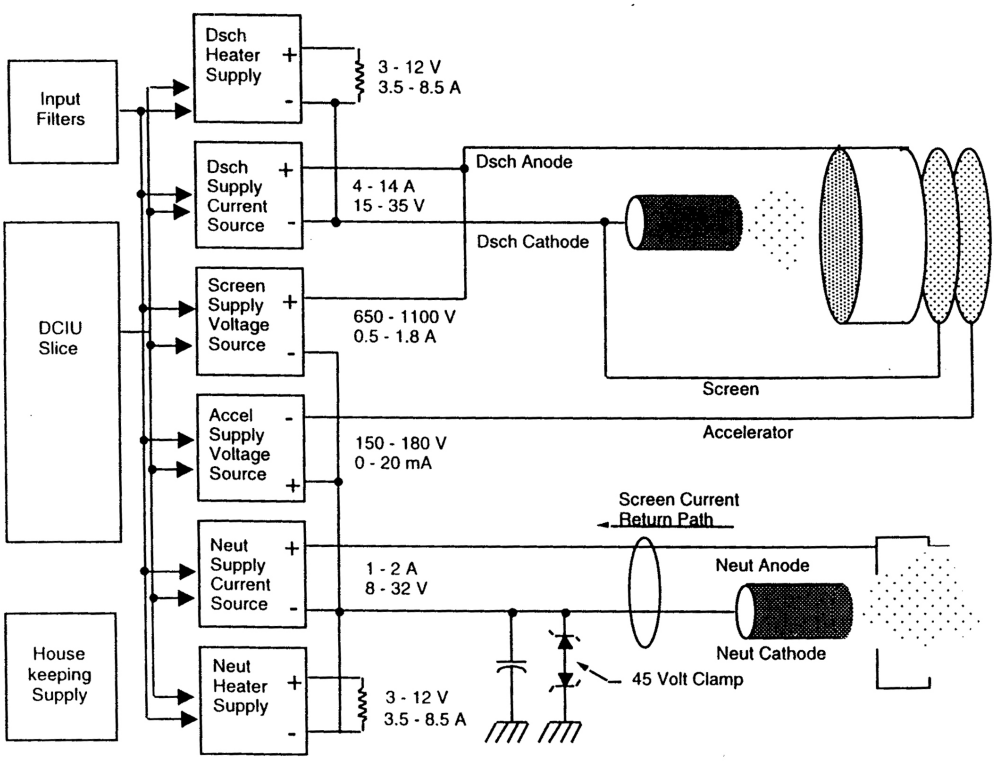

Figure 3. PPU−Block Diagram

Table 2. PPU Power Supply Requirements

Power Supply	Parameter
Beam Power Supply	
Output Voltage	650 to 1100 VDC
Output Current	0.5 to 1.8 ADC
Regulation Mode	Constant Voltage
Ripple	< 5% of Setpoint, Regulated Parameter
Accelerator Power Supply	
Output Voltage	–150 to –180 VDC
Output Current	0 to 0.02 ADC, 0.2 A surge for 100 ms
Regulation Mode	Constant Voltage
Ripple	< 5% of Setpoint, Regulated Parameter
Discharge Power Supply	
Output Voltage	15 to 35 VDC
Output Current	4 to 14 ADC
Regulation Mode	Constant Current
Ripple	< 5% of Setpoint, Regulated Parameter
Neutralizer Power Supply	
Output Voltage	8 to 32 VDC
Output Current	1 to 2 ADC
Regulation Mode	Constant Current
Ripple	< 5% of Setpoint, Regulated Parameter
Discharge Cathode Pulse Igniter	
Pulse Amplitude	650 V peak
Pulse Duration	10 μs
Rate of Rise	150 V/μs
Repetition Rate	10 Hz minimum
Discharge Cathode Pulse Igniter	
Pulse Amplitude	650 V peak
Pulse Duration	10 μs
Rate of Rise	150 V/μs
Repetition Rate	10 Hz minimum
Discharge Cathode Heater Supply	
Output Voltage	2 to 12 VDC
Output Current	3.5 to 8.5 ADC
Regulation Mode	Constant Current
Ripple	< 5% of Setpoint, Regulated Parameter
Neutralizer Cathode Heater Supply	
Output Voltage	2 to 12 VDC
Output Current	3.5 to 8.5 ADC
Regulation Mode	Constant Current
Ripple	< 5% of Setpoint, Regulated Parameter

discharge-power supply is then commanded to a current of 4.0 A, which is sufficient to vaporize small flakes of conductive material that may be shorting the accelerator system. The flight PPU mass listed in Table 1 includes 1.7 kg for micrometeoroid shielding.

2.1.4 Digital Control and Interface Unit (DCIU)—The DCIU, built by Spectrum Astro, Inc., serves as the data acquisition, control, and communications unit in the IPS and is packaged in a box designed to bolt onto the exterior of the spacecraft. The functions of the DCIU include: acquisition, storage, and processing of the signals from the sensors on the XFS and telemetry from the PPU slice; control of the valves in the XCA; control of the power supplies in the PPU (through the slice), and communication with the spacecraft data-and-control system. The DCIU executes stored sequences that control IPS-operating modes in response to high-level commands generated on the ground or autonomously by the spacecraft. The DCIU is powered by the 28-VDC spacecraft auxiliary-power bus and contains three half-width VME boards that perform the data acquisition, communications and processing, and valve-drive functions. The communications with the PPU slice occur over an RS422 interface; telemetry commands are

transmitted to the spacecraft on a MIL-STD-1553 interface. The mass of the DCIU shown in Table 1 does not include the weight of the thermal-control hardware provided by the DS1 spacecraft.

2.2 Key Technology-Validation Objectives

There are two key objectives of the NSTAR project:

1. Provide the information necessary to allow a project manager to baseline solar-powered ion propulsion technology on a spacecraft.
2. Stimulate commercial sources of, and uses for, ion-propulsion technology.

The NSTAR Project was started in 1992 to meet these objectives. Ion-propulsion technology had been under development in the laboratory for several decades, yet had never been included in a planetary or Earth-orbital mission application. While there are several different forms of electric propulsion thrusters, the NSTAR electrostatic ion engine design originated in 1960 when Harold Kaufman designed and tested the first broad-beam, electron-bombardment ion engine at NASA's Lewis Research Center (now NASA's Glenn Research Center). Early models of ion thrusters used Cesium or Mercury as propellant; demonstration models were flown in 1964 and 1970 on SERT I and II, among others [3]. While these flights showed that such thrusters could operate in space, they did not show that the thruster system could be built and tested with the reliability standards necessary for a flight mission or that the thruster could demonstrate the lifetime necessary for typical mission applications. Therefore, the NSTAR Project was initiated to validate this technology using a two-pronged approach: a ground-test program that was aimed at validating the full lifetime of the ion engine for future missions and a flight-test program that had the objective of demonstrating the delivery, integration, launch, and operations of flight-quality hardware and software. The overall objective of the entire effort was to produce the test-and-operational data that would allow a future spacecraft project manager to baseline this electric-propulsion system.

From these principal objectives, the NSTAR project developed and prioritized a list of derived objectives using a Quality Functional Deployment (QFD) technique. A QFD report was published May 2, 1995 [4]. This report described in detail the NSTAR QFD process. Many project stakeholders, including sponsors, scientists, and spacecraft managers, must have confidence in ion propulsion for it to be used. The NSTAR Project used QFD to merge the needs of a diverse set of stakeholders into a detailed list of technical requirements. Specifically, QFD allowed NSTAR to focus on the most important tasks as viewed by the future users of SEP. A summary of the prioritized QFD-derived objectives for the NSTAR project is given in Table 3 (with a high rating corresponding to a higher priority).

2.3 Expected Performance Envelope

The expected end-of-life (EOL) performance for the NSTAR IPS is specified at the 16 discrete-throttle levels shown in Table 4. These EOL values were developed based on the 8,000-hr life test of an engineering-model NSTAR engine [5,6].

Power throttling over the 16 NSTAR throttle-level settings is accomplished by varying the beam current at constant-beam voltage for throttle levels from 2 through 15. For NSTAR throttle levels 0 and 1, both the beam current and beam voltage are reduced. This throttling strategy maximizes the engine-specific impulse and efficiency at each power level. The engine-throttling envelope capability (with lines of constant-beam power) is shown in Figure 4. The upper boundary of this envelope represents the allowable maximum-beam voltage; the right-hand boundary represent the maximum allowable beam current. The lower boundary is determined by the ion-extraction capabilities of the ion-accelerator system and represents the minimum beam voltage that the engine can be operated at for a given beam current.

The minimum beam-voltage limit for a given beam current is called the "purveyance limit." The left-hand boundary represents the minimum beam current and is determined primarily by the minimum allowable discharge current. The minimum discharge current is a function of the cathode thermal characteristics. For the NSTAR engine, the minimum discharge current is 4.0 A, resulting in a minimum beam current of 0.5 A. The NSTAR throttle table was designed to run along the top of the engine throttling envelope to maximize the specific impulse and maximize the voltage margin between the beam voltage set point and the purveyance limit. This has the effect of minimizing the thrust at each power level. Other throttling strategies are possible; however, the potential benefits of alternate throttling strategies are highly mission specific.

The second column in Table 4 indicates the "Mission Throttle Level." There are 111 mission-throttle levels even though there are only 16 NSTAR throttle levels. These "extra" throttle levels result from specifying 6 new throttle settings between each NSTAR throttle level. These new "finer" throttle settings are used to take better advantage of the available onboard power and are achieved by reducing the beam voltage in 6 steps of 20 V each at constant beam current between each of the NSTAR macro-throttle levels.

2.4 Detailed Description

More detailed descriptions of the NSTAR hardware may be found in References [2, 5 to 18].

Table 3. Derived Objectives from the QFD Process

Customer Attributes	Rating
Low Life-Cycle Cost	9
Enhance US Industrial Competitiveness	9
Minimum SEP impact on Science Instruments	7.4
Short Interplanetary Cruise	7.4
Low Risk of Ion Propulsion Failure	7
Demonstrated Compatibility of SEP with Spacecraft	7
Compatibility With Small Spacecraft	7
Benefit to Successive Missions	7
Demonstrated Integration and Test of Ion Propulsion	6.4
Maximize Spacecraft Resources for Payload	6.4
Acceptable Development Cost Profile	6
Short Development Cycle	6
Low SEP Recurring Cost	5.6
System Reliability Quantified	5.6
Minimize Tracking Requirements	5.6
Minimal Development Risk	5.4
Simple/Proven Spacecraft Operation	5.4
Multiple Launch Opportunities	5.4
Minimal Cost Uncertainty	5
Minimal Development Schedule Uncertainty	5
Good In-Flight Recovery Options	4.6
Minimize Long Duration Ground Tests	4.4
Capture of Large Mission Set	4
Low-Cost Launch Vehicle	3
Minimize MOS Resources	2.6
Low SEP Non-Recurring Cost	2.4
Flight Heritage of SEP Hardware	2.4
Use Off-the-Shelf Components	1

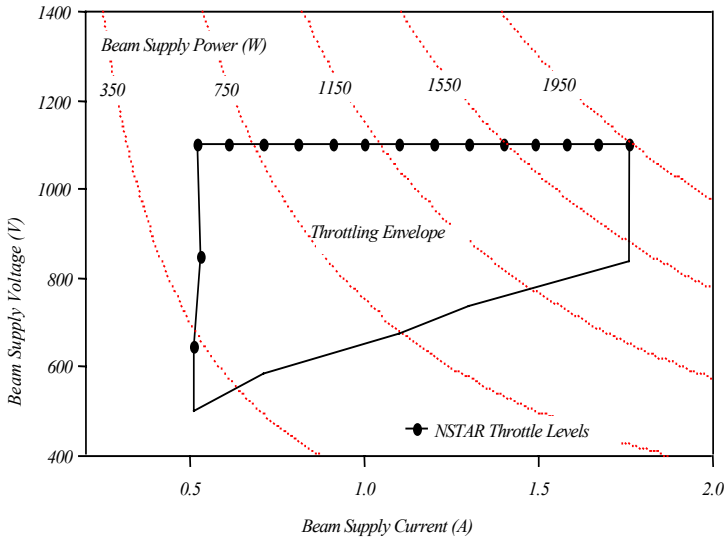

Figure 4. NSTAR Power-Throttling Strategy

Table 4. Table of Expected End-of-Life Performance

NSTAR Throttle Level	Mission Throttle Level	PPU Input Power (kW)	Engine Input Power (kW)	Calculated Thrust (mN)	Main Flow Rate (sccm)	Cathode Flow Rate (sccm)	Neutralizer Flow Rate (sccm)	Specific Impulse (s)	Total Thruster Efficiency
15	111	2.567	2.325	92.67	23.43	3.70	3.59	3127	0.618
14	104	2.416	2.200	87.87	22.19	3.35	3.25	3164	0.624
13	97	2.272	2.077	83.08	20.95	3.06	2.97	3192	0.630
12	90	2.137	1.960	78.39	19.86	2.89	2.80	3181	0.628
11	83	2.006	1.845	73.60	18.51	2.72	2.64	3196	0.631
10	76	1.842	1.717	68.37	17.22	2.56	2.48	3184	0.626
9	69	1.712	1.579	63.17	15.98	2.47	2.39	3142	0.618
8	62	1.579	1.456	57.90	14.41	2.47	2.39	3115	0.611
7	55	1.458	1.344	52.67	12.90	2.47	2.39	3074	0.596
6	48	1.345	1.238	47.87	11.33	2.47	2.39	3065	0.590
5	41	1.222	1.123	42.61	9.82	2.47	2.39	3009	0.574
4	34	1.111	1.018	37.35	8.30	2.47	2.39	2942	0.554
3	27	0.994	0.908	32.12	6.85	2.47	2.39	2843	0.527
2	20	0.825	0.749	27.47	5.77	2.47	2.39	2678	0.487
1	13	0.729	0.659	24.55	5.82	2.47	2.39	2382	0.472
0	6	0.577	0.518	20.69	5.98	2.47	2.39	1979	0.420

2.5 Technology Interdependencies

The ion propulsion system effects the design and performance of many other spacecraft subsystems as well as the mission operations. These subsystems include the solar array, the spacecraft power subsystem, thermal control, attitude control, communications, science instruments, command & control, and navigation. Part of the validation effort was to investigate and measure, if possible, the IPS direct effects on each of these systems.

2.5.1 Power System—The operation of the ion propulsion system is intimately coupled to the spacecraft power system. The IPS is by far the largest load on the power system. The power subsystem is designed to allow the battery to support occasional spacecraft loads during IPS thrusting. This enables IPS operation under transient and short-term negative power-margin conditions that maximizes power utilization. The spacecraft-power system is composed of:

1. A 2500-Watt (@1 AU solar range) concentrator solar array (SCARLET) power source.
2. Two 12-amp-hour (@ ~32 V) batteries to supply energy during power short falls.
3. An high-voltage power conditioning unit (HPCU) that supplies low-voltage power, controls the battery charge and discharge, and adjusts for changes in peak-power voltage.
4. A power distribution unit (PDU) to distribute and switch power.

The solar-array output and the high-voltage bus are tied together and have a voltage range from 80 V to 120 VDC.

To provide maximum power to the IPS during the thrusting phase, the spacecraft has to operate near the peak power point (PPP) of the array. The spacecraft requires a predetermined minimum level for each mission phase. Based on a projected PPP voltage, an uplink command is sent to the HPCU to have the array's operating-voltage set point selected slightly greater than the expected PPP. The set-point selection is updated every week during spacecraft tracking.

The IPS is commanded to a throttle level that corresponds to the maximum projected power from the array minus the expected spacecraft power consumption. If the battery is projected to discharge too deeply (defined as reaching 65% State of Charge (SOC) in about 30 minutes), an onboard software algorithm sends an autonomous command to IPS to throttle back one step.

The DS1 flight has shown that although the PPU with a thruster load generated some noise on the high-voltage bus, the high-voltage power-converter unit performed in a stable manner. The design of the HPCU on DS1 allows both the spacecraft avionics and ion propulsion to operate in a stable manner near the PPP of the solar array. This approach relies on a fairly well-defined solar-array model to determine the projected PPP. DS1 demonstrated that collapsing the solar-array voltage (pulling a larger load than was sustainable, resulting in an under-voltage condition) did not damage either the HPCU or the PPU. Onboard flight tests indicate that the HPCU can operate at a set-point voltage greater than the voltage corresponding to the PPP without collapsing the array voltage as long as the battery is capable of handling the needed power. The noise observed on DS1's high-voltage bus during normal operation is a function of the grounding configuration. A single-point ground approach was used for power-return lines on the spacecraft

with the star ground near the power source. The observed noise could be minimized on future spacecraft through improved routing of ground lines and shields.

2.5.2 Thermal—During IPS operation, the PPU can dissipate up to 200 Watts at 80° C. The top plate of the spacecraft (+Z axis) was used as the PPU and spacecraft's thermal radiator. The plate could radiate 235 Watts at 80° C and 85 Watts at 0° C. The PPU was designed to operate with baseplate temperatures between –5° C and 50° C with survival-temperature limits of –25° C and 55° C. The PPU was temperature controlled using a combination of 70- and 100-W heaters when not operating. During thrusting, the internal dissipation of the PPU maintains the PPU temperature, with the heaters being required only for operation at the lowest throttle levels. To minimize the power needed to heat the PPU at low throttle levels, the PPU temperature is kept near the lower limit allowed for normal operation.

The DCIU temperature is heater controlled and presents a constrained thermal load to the thermal system. The changing solar aspect angle is the chief driver to a change in thermal operation. The DCIU is designed to operate from –15° C to 50° C with survival limits of –25° C to 55° C.

The XFS temperature is also heater controlled. To minimize the power needed to heat the XFS, the XFS temperatures are kept near the lower limit of normal operation. The flow-control devices are kept above 20° C to maintain their calibration. The Xe propellant tank is kept between 20° C and 50° C to maintain the super-critical gas state while not over pressurizing the tank.

The thruster is placed inside the conical launch-vehicle adapter within the gimbal rings as shown in Figure 5. During normal IPS operation, the thruster is self-radiating and no additional thermal control is required. The waste heat from the thruster is isolated from the spacecraft and blocked by the gimbal rings and adapter. Consequently, the only significant thermal emission is in the -Z axis (thruster plume direction). The thruster is buried in the launch vehicle adapter such that only the neutralizer is in sunlight when the Sun is perpendicular to the -Z axis. This minimizes the solar load on the thruster. When the Sun is in the -Z axis hemisphere, the solar load increases significantly. To keep the solar load from over heating the thruster magnets, the Sun was not permitted to go closer than 30 degrees to the -Z axis when the thruster was operating at a high power and 1 AU from the Sun.

2.5.3 Attitude Control—The initial and continuous control of the IPS thrust vector was an important IPS validation activity because of its potential to impact the spacecraft's attitude-control subsystem. When the IPS was not thrusting, 3-axis control of the DS1 spacecraft was accomplished using a blow-down hydrazine system. Each of the three-axis dead bands was controlled to various levels depending upon the mode of operation and hardware constraints. The dead bands were tightened when imaging and loosened to save propellant when in an IPS thrusting or non-thrusting cruise mode.

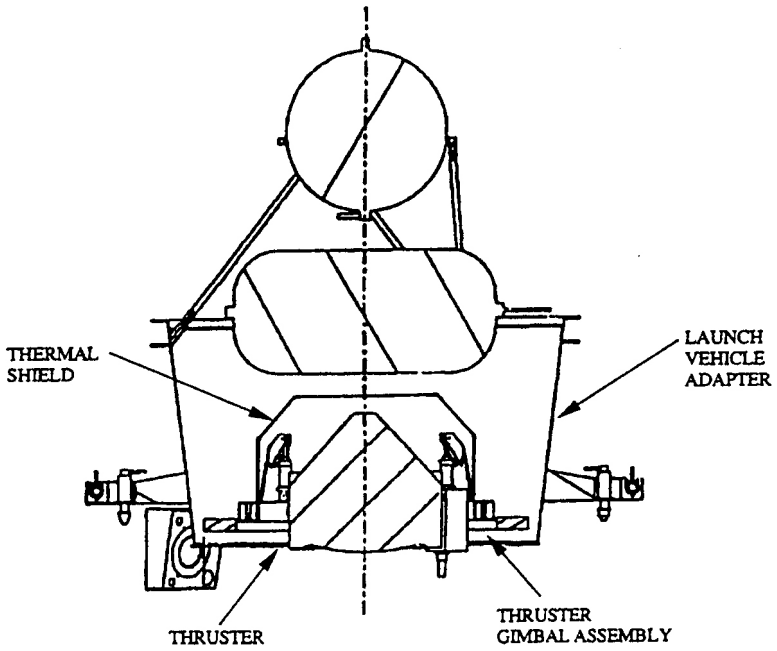

Figure 5. NSTAR Thruster Thermal Environment on DS1

When starting the IPS, the 3-axis dead bands are set to ±1 degree. This is done to ensure that attitude control is maintained when stabilizing the control loop during thruster start. After the engine is started, the ACS gimbal is slewed ±1 to 2 degrees to measure the IPS control torque. Gimbal slews during the initial IPS start up are given in Figure 6a and Figure 6b. This slew procedure is also performed during IPS recycles (indicated by the solid circles) and can be seen following the solid circle just before 1 AM. The slew algorithm during recycles was suppressed later in the mission since the recycles are very short and do not change the gain of the control loop. Note that the thrust level at mission level 6 (NSTAR Throttle Level 0) is only 20 mN and requires the smallest control authority. The attitude-control loop operation was validated for IPS thrust from 20 mN to 78 mN during the initial acceptance test.

The gimbal controller is used to center the thrust through the spacecraft center of mass and maintain the spacecraft attitude along the spacecraft X- and Y-axis. The Z (roll) axis is maintained by the hydrazine thrusters. The X- and Y-axis thruster do not fire once the control loop is stabilized.

Periodically the spacecraft orientation is changed as the gimbal angle deviated from zero degrees. This is done to compensate for a shift in the spacecraft center of mass. The thruster, spacecraft, hydrazine tank, and xenon propellant tank, however, were centered extremely well, eliminating the need for this compensation. Further, the gimbal potentiometer became very noisy as the mission progressed causing an erroneous pointing of the thrust vector. The potentiometer was eliminated from the control loop later in the mission.

Two stepper-motor drives are used to control the gimbal position and can slew the gimbals +6 degrees before running into the mechanical stops. The data from DS1 suggests that the gimbal travel could have been limited to +2 degrees.

The spacecraft attitude-control system (ACS) consumes about 7 grams of hydrazine per day when the IPS is on. In this mode the spacecraft ACS uses the:

- IPS and gimbals to obtain 2-axis control.
- Reaction control subsystem (RCS) to control:
  - The third axis.
  - All major turns.

When IPS is off, spacecraft consumes about 10 grams of hydrazine per day, and the ACS uses the RCS to control:

- The three axes.
- All major turns.

The approximate propellant consumption required for various operations is given in Table 5. Note that the effect of solar distance is ignored.

Table 5. Approximate Hydrazine Consumption Per Activity

RCS Activity	Average Propellant Consumption (gram/day)
IPS thrust on with no OpNav	7
IPS thrust on with 1 OpNav per week	15
IPS off with no OpNav	9.7
OpNav	52
Spacecraft turn to vector	40

2.5.4 Science Instruments—No interference has been observed by the remote sensing instruments when the IPS is thrusting. This was validated by the miniature integrated camera and spectrometer (MICAS) instrument when 3 CCD, 3 APS, 3 IR, and 3 UV exposures were taken with IPS off followed by a second 3 CCD, 3 APS, 3 IR, and 3 UV exposures taken with the IPS on. The IPS was operating at 1 kW with the MICAS pointing well away from the Sun to minimize solar reflection. The results, shown in Table 6, indicate that there is no impact of IPS operation.

The particle and field measurement sensors were mildly affected by the IPS. With the IPS off, the magnetometer from the IPS Diagnostics System (IDS) was used to measure the thruster's magnetic field. The thruster magnetic field was observed to vary as the gimbal/thruster was rotated. With the IPS on, the IDS magnetometer was able to see the variation in the thruster-produced magnetic field due to the motion of the gimbal/thruster, a change in the thruster power, and variations in the thruster's magnet temperature. Future magnetometers can correct for the IPS' magnetic field by incorporating a conventional boom and inboard and outboard magnetometers.

The plasma experiment for planetary exploration (PEPE) instrument was able to measure residual xenon using a mass spectrometer. Future sensors using high-voltage accelerator/ detectors may find it necessary to filter the xenon line in their spectra. However, operating the IPS did not interfere with PEPE's solar-wind measurement.

2.5.5 Communications—The radiative- and conductive-electromagnetic interference of IPS upon the spacecraft and instruments appears to be extremely small. The only interference noted was an increase in telemetry-system noise, mostly due to a spacecraft's ground loop. X-band transmission through the IPS plume was performed at various angles and IPS power levels. No significant effect

Table 6. MICAS Image-Noise Comparison with the IPS On and Off

IPS State	Star Field	Micas Sensor	Exposure (S)	Pixels or Elements	Minimum Level (dn)	Maximum level (dn)	Mean Signal (dn)	Standard Deviation (dn)
off	1	CCD	0.218	1064960	107	576	134	5.18
on	2	CCD	0.218	1064960	107	283	135	5.16
off	1	CCD	1.750	1064960	106	1025	136	7.27
on	2	CCD	1.750	1064960	104	1002	136	7.20
off	1	CCD	9.830	1064960	106	3284	149	45.80
on	2	CCD	9.830	1064960	105	3248	150	45.30
off	1	APS	0.874	65534	97	158	122	2.93
on	2	APS	0.874	65534	98	153	122	2.69
off	1	APS	1.750	65534	89	155	123	2.71
on	2	APS	1.750	65534	89	159	122	2.86
off	1	APS	4.920	65534	97	151	121	2.83
on	2	APS	4.920	65534	97	154	122	2.91
off	1	IR	0.874	139392	0	3515	287	168.00
on	2	IR	0.874	139392	0	3525	288	168.00
off	1	IR	3.500	139392	0	3512	291	171.00
on	2	IR	3.500	139392	0	3529	291	172.00
off	1	IR	9.830	139392	0	3519	297	176.00
on	2	IR	9.830	139392	0	3526	297	177.00
off	1	UV	4.920	20020	723	815	785	24.60
on	2	UV	4.920	20020	713	805	776	24.10
off	1	UV	14.000	20020	726	950	893	58.40
on	2	UV	14.000	20020	716	946	884	57.90
off	1	UV	28.000	20020	735	1168	1070	95.20
on	2	UV	28.000	20020	723	1165	1060	97.70

was noted during any of the tests. Figure 7 shows that there is no discernible difference in signal to noise when the IPS was throttled at NSTAR level 0, 1, 2, 3, and 4 (500 to 1000 Watts) and from when the IPS was not on. During this test, the low-gain antenna was used for two-way Doppler through the IPS plume, which was pointing at the Earth, and the DSS 55 Block V receiver was used in right-hand circular polarization operating at 8.42 GHz. The vertical scale on Figure 7 is from 12 to 21.3 dB, while the horizontal scale covers from DOY 148 14:37 to 23:15. Note that the IPS was operating at NSTAR throttle level 0 for more than 7 hours before this test to ensure that the thruster was operating in steady state xenon-flow conditions.

2.5.6 Command & Control—The IPS command, control, and telemetry were made very simple to ensure that the integration of IPS to the spacecraft was uncomplicated and the operability by the MOS team straightforward. The basic commands used during normal thrusting were Safe, Standby, Thrust On, Thrust Off, and Throttle Level. A few other commands were used to: initially start up the DCIU, power on the DCIU, perform special diagnostic tests, initially prepare the IPS after launch, and prepare IPS for startup. The control of the IPS was automated so that no monitoring was needed.

The IPS telemetry stream from the DCIU to the spacecraft was composed of a data packet containing all measured IPS parameters sampled every second. This maximum quantity was often filtered by the spacecraft's telemetry manager to packets each 2 seconds, each 5 seconds, each 5 minutes, etc., in length for insertion into the downlink because of data management issues on board and the robustness of the telemetry link with the ground. IPS data volume was high during critical operating times, such as engine start, and was lower during cruise operations.

2.5.7 Mission Design and Navigation—The DS1 mission design and navigation teams demonstrated that IPS can be reliably flown to multiple planetary targets. Further, the teams have demonstrated that autonomous operation is possible. Since DS1 was the first low-thrust mission, a number of processes had to be modified, tested, and integrated. The first category of process was comparable to conventional mission-design and navigation software:

- Preliminary trajectory-design.
- Intermediate trajectory-design.
- Ground-navigation.

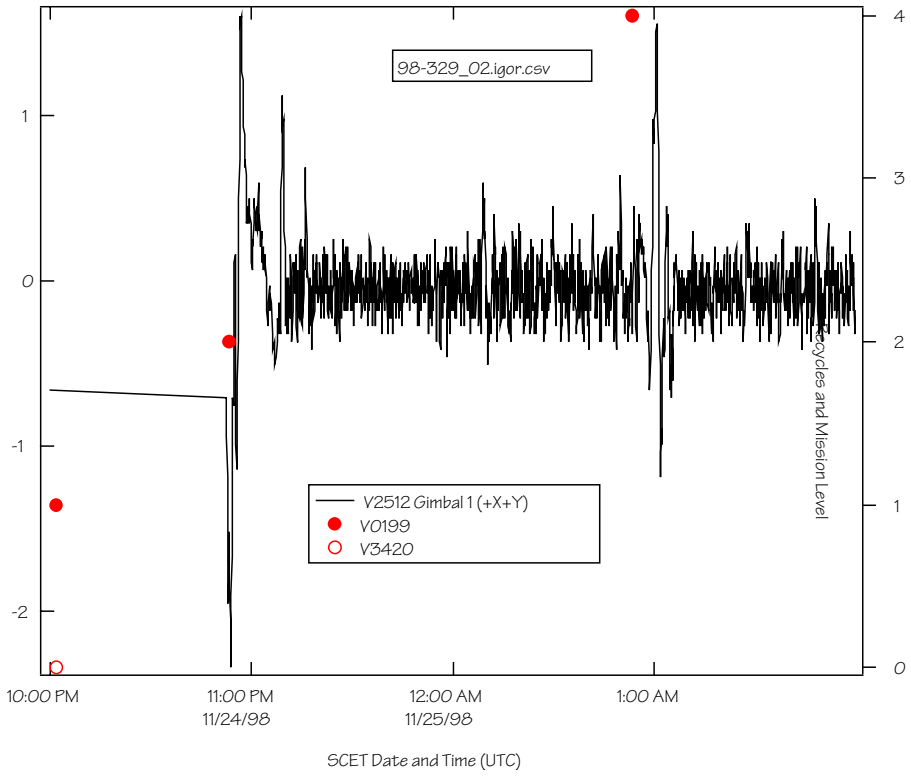

Figure 6a. Gimbal 1 Slew at Start Up and Recycle @ Mission Level 6

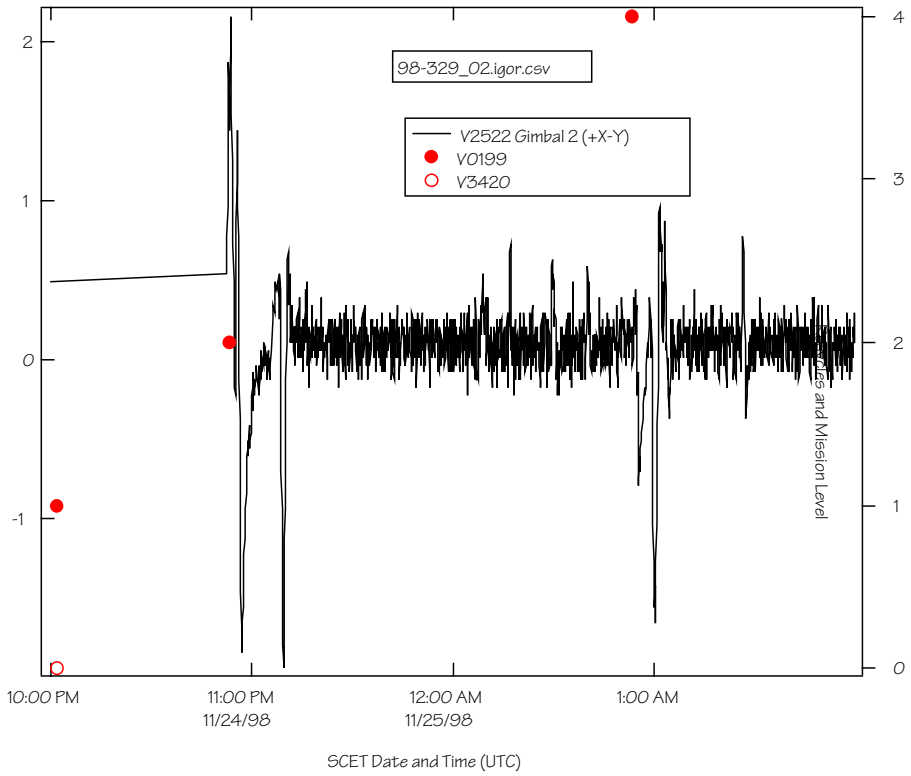

Figure 6b. Gimbal 2 Slew at Start Up and Recycle @ Mission Level 6

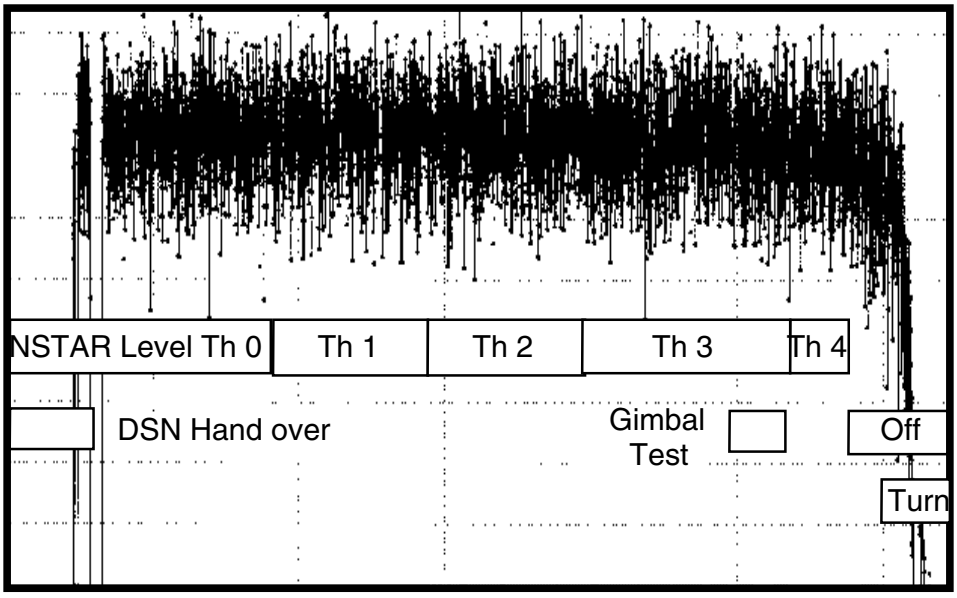

Figure 7. IPS Acceptance Test 2, X-Band Signal to Noise

To implement autonomous navigation, a number of other processes had to be developed, tested, and integrated. These can be put into three autonomous software categories:

- Orbital determination.
- Trajectory design.
- Command and control.

The low-thrust trajectory program that was used to develop the preliminary heliocentric trajectory neglects the Earth's mass. To refine the trajectory it was necessary to propagate the launch trajectory using a trajectory program that includes the Earth's gravity. By propagating the trajectory out of the Earth's gravitational sphere of influence and determining the spacecraft's state at that point, a starting point was used to begin the low-thrust trajectory program.

The available IPS power over the mission is required for trajectory optimization. This requires that the solar array and spacecraft's power be defined as a function of solar distance, aging, and radiation-dose. The solar-array power changes as a function of solar-array temperature, aging, and the spacecraft's load characteristics. The spacecraft's power changes as a function of solar distance, and aging, which changes the amount of heater power required to maintain subsystem temperatures.

During the flight of DS1, the trajectory was re-optimized to take into account changes in thrusting profiles. Whenever the original IPS thrust profile was not followed, the trajectory was re-optimized and re-planned with very little performance penalty. In addition, DS1 demonstrated that thrusting does not necessarily need to be in the optimal direction. Many times during the DS1 mission, the thrust was pointed in a direction defined by the convenience of the mission, instead of the optimal trajectory direction, without a significant penalty.

The mission-design process resulted in a linearized trajectory indicating the trajectory state, thrust, and thrust direction on one-day centers. The trajectory incorporates the effects of thrust-duty cycles, coast periods, and periodic hydrazine drop-off mass. The navigation team used this as a preliminary trajectory to begin the detailed navigation trajectory development.

DS1 used a low-thrust trajectory program called SEPTOP for the preliminary mission design. The program inputs are models of power (solar range, aging, and radiation dose), IPS performance (thrust and mass flow as a function of IPS input power), spacecraft power (as a function of solar range), and initial launch state (position, velocity, and mass) away from the gravitational attraction of Earth. The models for IPS performance are continuous and characterized in SEPTOP as coefficients of a fourth-order polynomial. When the program has an optimal solution, it outputs the power level, thrust, thrust direction, mass flow, and spacecraft state in 1-day increments. Because the inputs into SEPTOP are continuous curves (as defined by the polynomials), the output is also continuous. However, since the IPS has quantized operation, this translation must be done by the navigation software (auto-navigation). The IPS–mission, throttle–table values are used by auto-navigation to select the proper throttle profile (throttle level) over the mission after trajectory has been optimized by SEPTOP. The mission throttle table uses the end-of-life (EOL) value for power, flow rate, and thrust. The mass flow rate and thrust do not change as the thruster ages, so only the IPS input power increases with thruster age.

Computer Algorithm for Trajectory Optimization (CATO) is an intermediate-level trajectory program that could add further fidelity to the trajectory design. It has the capability of adding the gravitational effects of the Earth and the Moon. CATO was used to generate the launch state used by SEPTOP. It was also used to test the fidelity of the SEPTOP trajectory. It was found that the optimization process using a detailed trajectory design was time consuming and did not offer any major benefits.

There are three major navigation tasks: 1) convert the preliminary trajectory received from mission design into a detailed flyable trajectory, 2) determine the current spacecraft and target state (position and velocity) using Doppler, ranging, and optical navigation, and 3) determine the maneuver file needed to fly to the target.

The flight-navigation software is important to IPS validation because in addition to the control of the IPS thrust level and spacecraft thrust vector, it is used to autonomously plan maneuvers over the entire mission. The maneuver plan takes into account the effects of IPS-burn errors, spacecraft-pointing errors, solar pressure, and hydrazine attitude-control maneuvers.

There are a number of mission-margin elements, all of which are interrelated. The major elements are available IPS power, available xenon propellant, thrust profile, and thrust duty cycle. This is somewhat different than chemical propulsion systems, where propellant, interstellar probe (Isp), thrust, and burn time are mission margin elements.

The thrust duty cycle is used as the major control of mission margin. Instead of assuming in the trajectory design that thrusting occurs when permitted, each thrust segment is assumed to have a duty cycle less than 100%. A shortfall of thrust impulse would be corrected by increasing the duty cycle. The duty cycle used by DS1 varied from 90% to 92%. The remaining 8% to 10% is not all usable since a portion is used for optical navigation and downlink of data.

A second mission margin tool is the use of forced ballistic coasts during very efficient thrust periods. The trajectory design program is made to perform coasts during normally optimum-thrust periods. This results in a mission penalty. but ensures that an IPS anomaly that temporarily disrupts thrusting will not threaten the mission.

2.5.8 Contamination—Risking spacecraft contamination by the ion engine's non-propellant efflux has always impeded the use of ion propulsion. Consequently, the NSTAR project included since its inception the development of a diagnostics package of contamination-monitoring instrumentation to fly with the engine. The location of the NSTAR diagnostic package (NDP) instrumentation relative to the ion engine on DS1 is shown in Figure 8. The NDP contamination-monitoring instruments include quartz crystal microbalances (QCM) and calorimeters packaged together in a remote sensors unit (RSU). The RSU is located 75 cm from the centerline of the ion thruster's exhaust beam. One pair of contamination monitors (QCM0, CAL0) has a direct line-of-sight view of the ion engine's accelerator grid (~85° from the thrust centerline). The other pair (QCM1, CAL1) is shadowed from the ion engine's accelerator grid by the launch vehicle interface ring on the propulsion module assembly.

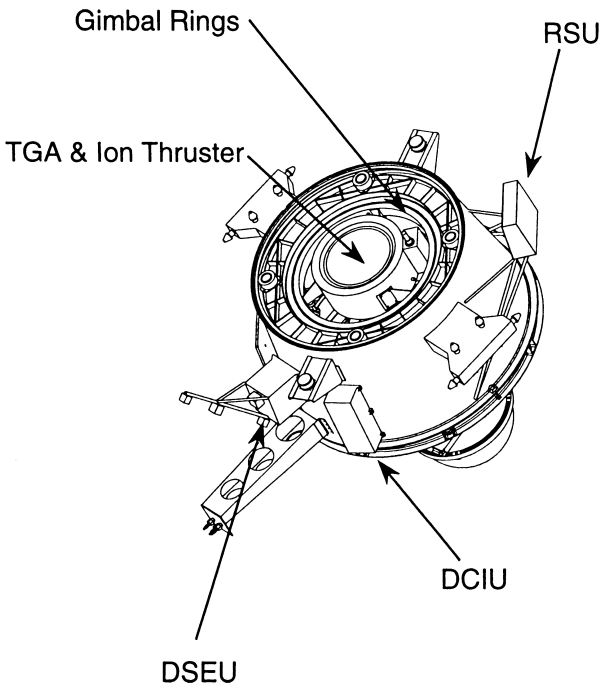

Figure 8. Location of Diagnostics Hardware on the DS1 Propulsion Module

The data from QCM0 and CAL0 are consistent with the collection of a total of 250 angstroms of molybdenum from launch through November 1999. These data have not been corrected for solar-illumination and temperature effects on the QCM beat frequency. However, these effects are believed to be minor for QCM0 because the observed change in frequency (Δf >5,000 Hz since launch) is much greater than either the solar-illumination effect (Δf <250 Hz shadow to maximum illumination) or the thermal effect (Δf <50 Hz for $\Delta T \leq 60°$ C in the range +20° C to +80° C). These effects are relatively more important for QCM1 since it has indicated Δf <500 Hz since launch.

Of the 250 angstroms of molybdenum collected by QCM0, 100 angstroms were collected in the first 750 hours of NSTAR operation. The deposition rate appears to be well correlated with the Mission Throttle Level, as indicated in Figure 9 and Figure 10.

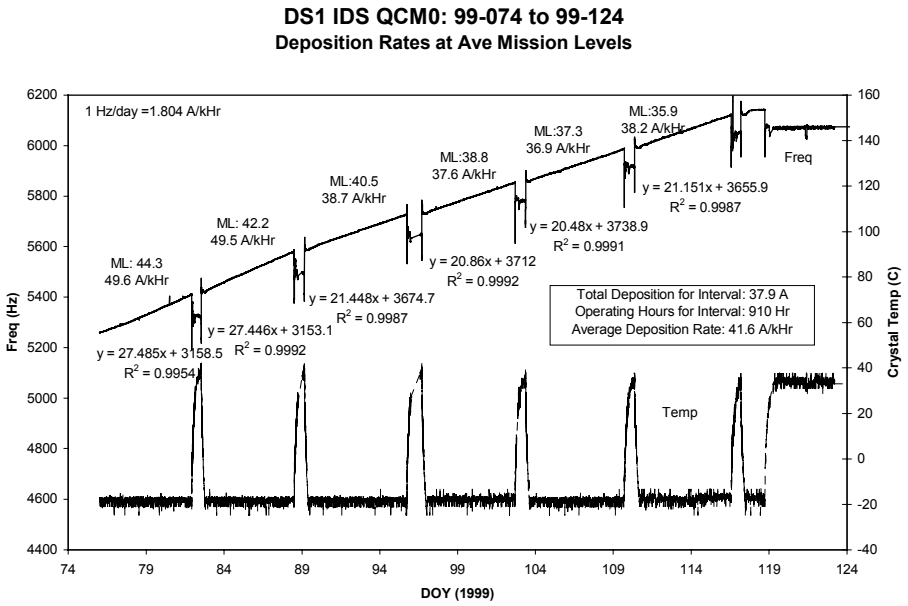

Figure 9. QCM Deposition Rate vs. Time and Mission-Throttle Level

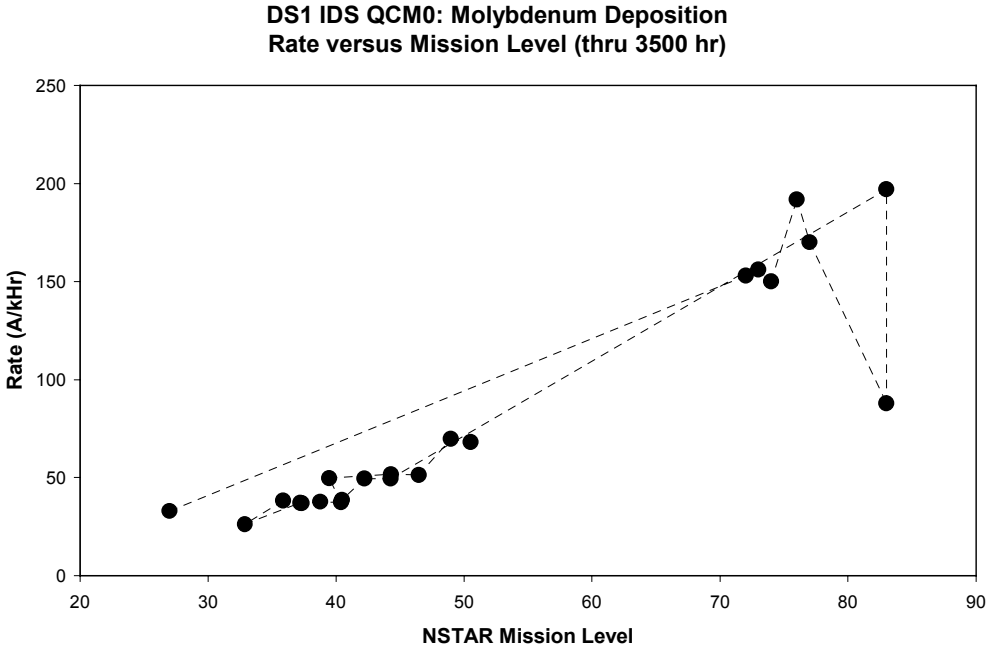

Figure 10. QCM Deposition Rate Increases with Mission-Throttle Level

Based on preliminary analyses of the results from the witness monitors from the 8,000-hr life demonstration test, it is estimated that the molybdenum collection rate during the ground test at the location corresponding to the position of QCM0 is approximately 160 angstroms/kWh. The average molybdenum collection rate for QCM0 on DS1 is 70 angstroms/kWh. Since the average engine power on DS1 is approximately half that of full power (the 8,000-hr test was run at full power) and since the grid erosion rates are expected to scale with engine power, it appears that ground test and flight test deposition rates are comparable.

2.6 Test Program

The NSTAR test program employed an extensive ground-test activity together with the flight test on DS1 to validate the ion propulsion technology.

2.6.1 Ground Test Program—The NSTAR ground-test program was planned around the use of engineering-model thrusters (EMT) build by NASA GRC and, eventually, flight model thrusters fabricated by HED. A total of four EMTs and two flight thrusters were fabricated and tested. The principal objective of the ground-test program was to demonstrate that the NSTAR thruster design had sufficient total-impulse capability and reliability to accomplish deep-space and near-Earth-space missions of near-term interest. The NSTAR project originally included a sequence of four major tests labeled NPT1 through NPT4, as indicated in Table 7. Between NPT1 and NPT3, however, the actual project ground-test history included three other series of tests termed development tests (DTs), engineering development tests (EDTs), and characterization tests (CTs). These test series were inserted into the NSTAR project in order to provide sufficient information to be confident that the NSTAR thruster and the NSTAR IPS designs would function as promised and with high reliability.

The long duration tests shown in Table 7 were designed to identify unexpected failure modes, characterize the parameters that drive known failure mechanisms, and determine the effect of engine wear on performance. The first test, NPT1, was planned to be 2,000 hours of operation at the full-power point. Failure of a non-flight-type propellant isolator resulted in the test being divided into two test segments: NPT1 and NPT1A. Several potential failure mechanisms were identified in these test segments (see References [17,18] for details). These failure mechanisms were studied in the subsequent shorter duration DTs listed in Table 8.

Table 7. NSTAR Project Tests (NPT)

Test	Purpose	Description	Thruster	Duration (hrs)	Xenon Throughput (kg)
NPT 1	Wear	First 2K	EMT1	867	9.4
NPT 1A	Wear	Finish 2K	EMT1	1163	12.6
NPT 2a	FIT A	PPU integration test	EMT2	21	N/A
NPT 2b	FIT B	PPU integration test	EMT3a	12	N/A
NPT 3	LDT	Life Demonstration Test	EMT2	8194	88
NPT 4	ELT	Extended Life Test	FT2	>12,000*	125*

*Planned

Table 8. NSTAR Development Tests

Test	Purpose	Description	Thruster	Duration (hrs)	Location
DT 1	erosion rate	floating & grounded Screen Grid (SG)	EMT1	37	GRC 5
DT 2	erosion rate	grounded SG	EMT1	50	GRC 5
DT 3	erosion rate	floating SG	EMT1	51	GRC 5
DT 6c	technq accuracy	floating SG–measurement accuracy	EMT1	0.25+	GRC 3
DT 7	mass loss	grounded SG	EMT1	100	GRC 3
DT 16	performance	new grids, backup badges	EMT1a	12	GRC 3
DT 9c	low power perf.	@ low power w/ margin testing	EMT1a	168	GRC 3
DT 18	perf. & margins	second part of old DT 17	EMT1b	50	GRC 5
DT 8a	facility check	with flow sensitivity	FMT	21	JPL148
DT 9b	low power perf.	@ low power w/ margin testing	FMT	870	JPL149
DT 15	revalidation	redesigns for NPT1 issues	EMT1b	1011	JPL148
DT 19	chamber check	replaces DT 17a	J-Series	24	JPL148

As a result of these tests several design changes were made to the engineering model thrusters. The effectiveness of these design changes in eliminating the failure modes identified in NPT1 was then validated in DT15 using EMT1b, which incorporated the design changes. This development test was planned to be a 1,000-hour wear test at the full-power point. Since the failure modes were originally observed in both of the approximately 1,000-hr long NPT1 test segments, the duration of DT15 was selected to be 1,000 hours, with the expectation that this was the shortest test duration that could provide confidence that the failure modes had been eliminated. It was essential to have this confidence prior to starting the endurance test for the full 8,000-hour design life. The development test DT15 was successfully executed and the test was voluntarily terminated after 1,011 hours of operation at full power. Post-test inspection of the thruster indicated that the design changes had successfully eliminated the failure modes observed in NPT1 [18].

2.6.1.1 8,000-hr Life Demonstration Test—Following DT15, the NSTAR project test NPT3, which was designed to demonstrate the full 8,000-hr thruster life, was carried out. This life demonstration test (LDT) used the second engineering-model thruster, EMT2, and was the most successful endurance test of a high-power ion engine ever performed (details of this test are given in [5,6]). A total of 8,192 hours of operation was achieved at the 2.3 kW full-power point before the test was voluntarily terminated. A total of 88 kg of xenon propellant was processed, demonstrating a total impulse of 2.73×10^6 N-s.

Thrust measurements taken over the entire-throttling range at the beginning of the test are shown with calculated beginning-of-life (BOL) values and calculated values at the end of the 8,000-hr test in Figure 11. The difference between the measured and calculated thrust is less than 1 mN. The calculated thrust is essentially constant as a function of time because the engine conditions that effect the thrust calculation are controlled. The total engine efficiency is given as a function of time over the 8,000-hr test for six throttle levels in Figure 12. These data indicate a slight decrease in engine efficiency over the first 4,000 hours of the test and very little efficiency change over the second half of the test.

Demonstrating adequate life of the neutralizer cathode was one of the key objectives of the 8,000-hr test. To achieve adequate service life of the neutralizer, its operation must be kept in what is referred to as the "spot mode." This mode of operation is characterized by a relatively low neutralizer-keeper voltage with low-amplitude voltage oscillations. The neutralizer can also operate in what is known as the "plume mode" characterized by a higher neutralizer-keeper voltage and higher amplitude-keeper voltage oscillations. Operation in the plume mode is believed to result in a significantly shortened neutralizer-service life. The operating mode for the neutralizer is determined by the flow rate for a given emission current. The neutralizer operation as a function of flow rate was characterized periodically over the entire throttling range to monitor changes in the flow-rate margin. A certain minimum flow rate and total-emission current are required to prevent plume-mode operation. The flow-rate boundary between stable spot-mode operation and plume mode for the neutralizer over the entire NSTAR throttling range is shown in Figure 13. The difference between the flow rate corresponding to the plume/spot mode boundary and the flow rate specified in the throttle table is the flow-rate margin.

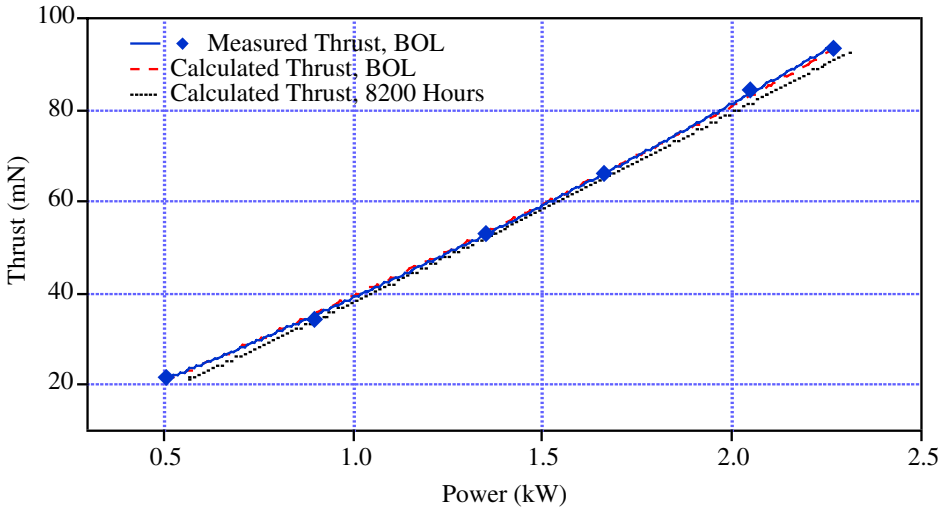

Figure 11. Comparison of Measured BOL Thrust with Calculated Thrust at BOL and EOL

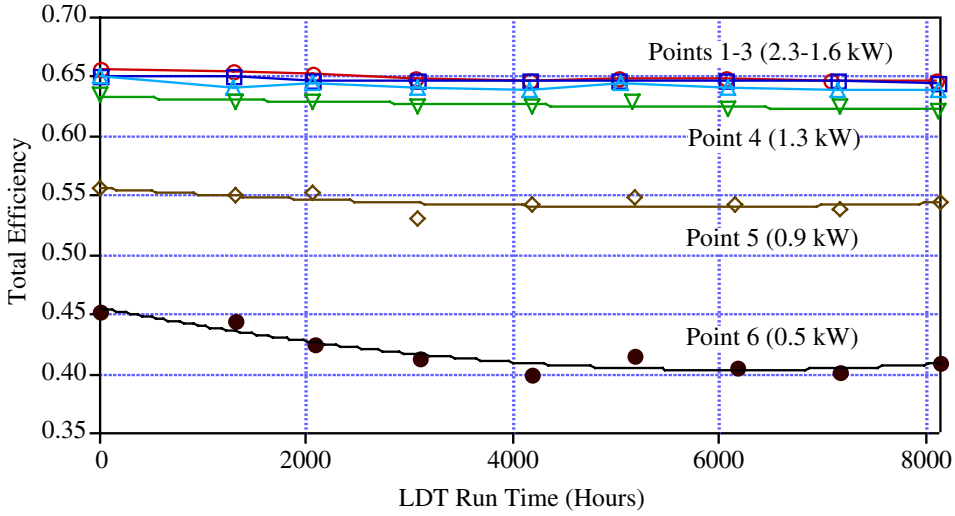

Figure 12. Engine Efficiency as a Function of Time and Power Level during the 8,000-hr Test of EMT2

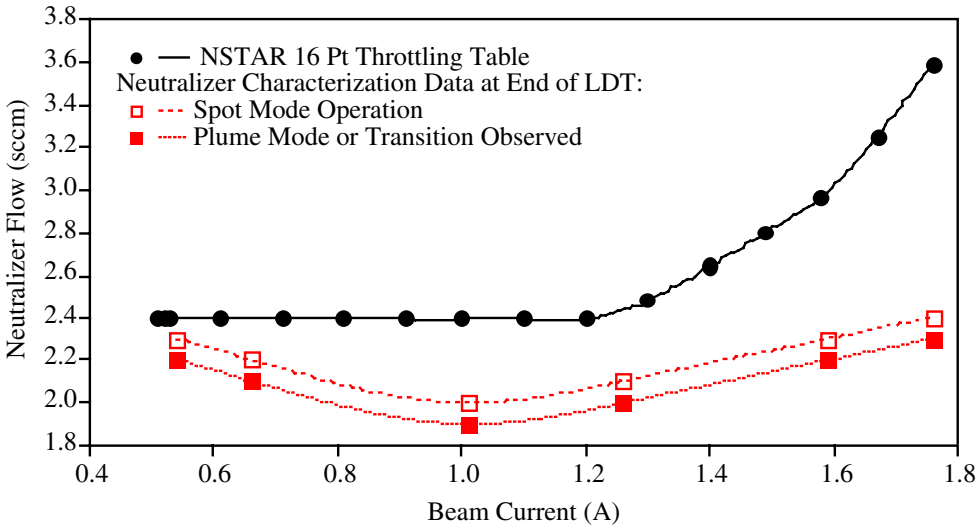

Figure 13. Margin Between the NSTAR Neutralizer Flow Rates and the Transition from Spot to Plume Mode

The neutralizer cathode was also disassembled and examined for signs of wear and material transport. The only significant wear site was the neutralizer-cathode orifice. The upstream-orifice diameter was essentially unchanged from the pretest value of 0.280 mm, while the downstream end of the orifice increased by 70 percent to 0.48 mm. The surface of the chamfer was observed to be heavily textured from ion bombardment, but no significant dimensional changes have occurred. Small tungsten deposits up to about 10 µm in diameter were found inside the orifice near the upstream entrance. The upstream face of the orifice plate showed no signs of erosion, although a ring of barium deposits was found around the orifice. There was only slight surface texturing on the downstream face of the cathode-orifice plate and no damage to the weld between the plate and the cathode tube.

The neutralizer-keeper electrode also experienced very little wear. The downstream face and weld show no evidence of sputter damage. The upstream face of the molybdenum keeper has a thin deposit of tungsten around the orifice; this might have come from the neutralizer orifice. A portion of the tantalum-keeper tube was exposed to high-angle-beam ions and shows some surface texturing, but no significant mass loss.

A number of ion-optics performance parameters were measured periodically during the 8,000-hr test at the

nominal- and throttled-operating points. After the test, the grids were examined for signs of wear, including sectioning and detailed SEM measurements of erosion-site geometry. The beam-current density and potential distributions measured about 2.5 cm downstream of the exit plane are shown in Figure 14 and Figure 15. The beam-current density distribution is strongly peaked on the centerline, but drops sharply at a radius of 12 to 13 cm, which is 1 to 2 cm radially in from the periphery of the hole pattern. These profiles did not change significantly over the test and yield average flatness parameters ranging from 0.32 at the minimum power point to 0.46 at full power. The peak-beam potential ranges from 3.2 to 4.9 V and is largest for intermediate power levels. Both distributions show peak offsets from the thruster centerline. This phenomenon was quite repeatable and evidently represents a true deviation from axis symmetry in the beam.

The 8,000-hr test identified electron-backstreaming as one of the key potential-failure modes for the engine. Electron-backstreaming refers to the phenomenon in which the space potential in the centers of the accelerator-grid apertures is insufficiently negative to prevent electrons in the beam plasma from streaming backwards into the engine. This phenomenon can result in a substantial performance loss for the engine, as well as the potential to damage the thruster by over heating. The accelerator-grid voltage at which electron-backstreaming occurs was measured periodically throughout the 8,000-hr test and is shown in Figure 16 for operation at the full-power point. The increase in the magnitude of the accelerator-grid voltage required to prevent electron-backstreaming observed over the 8,000-hr test results from the enlargement of the accelerator-grid apertures due to sputtering by charge-exchange ions. Post-test measurements of the accelerator-grid apertures as a function of the radial

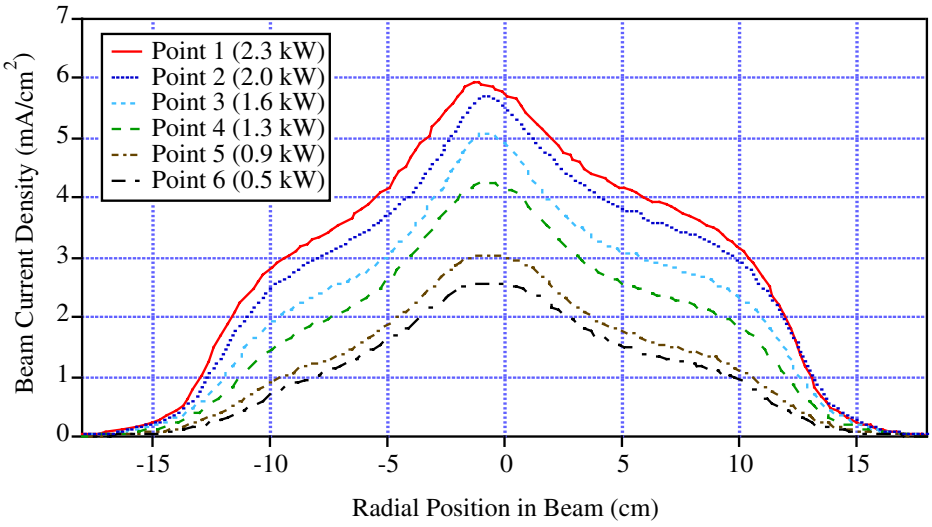

Figure 14. Beam Current Density Distribution Measured at BOL for Six Throttle Levels (EMT2)

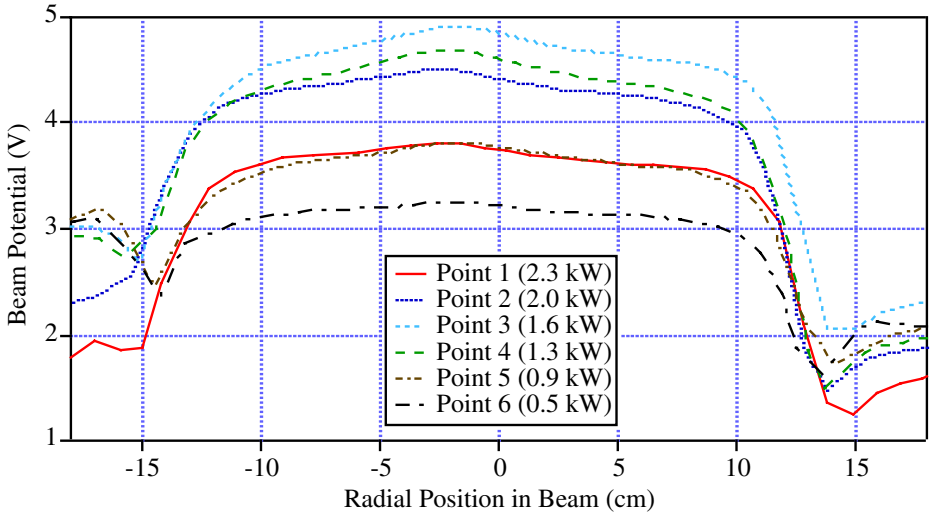

Figure 15. Beam Potential Measurements at BOL for Six Throttle Levels (EMT2)

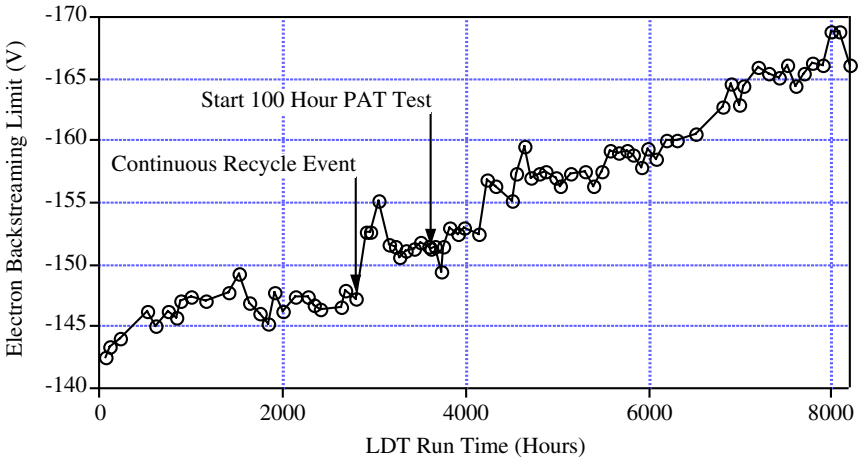

Figure 16. Variation in Electron-Backstreaming Voltage at Full Power over the Course of the 8,000-hr Test (EMT2)

position on the grid are given in Figure 17. The pre-test accelerator-grid-aperture diameters are 1.14 mm. These data indicate a significant increase in the aperture diameter in the center region of the grid. The electron-backstreaming voltage margin at the end of the 8,000-hr test is given in Figure 18 over the NSTAR throttling range. While these voltage margins appear to be small, the accelerator grid could easily be operated at voltages more negative than those in the throttle table late in the engine life with essentially no adverse effects. The NSTAR PPU can provide accelerator-grid voltages as negative as –250 V.

The 8,000-hr test also provided a wealth of information regarding the details of other potential wear-out modes, including: erosion on the downstream side of the accelerator grid, erosion of the screen grid, erosion of the cathode keeper electrode, erosion of the cathode-orifice plate, and the thicknesses of sputter-deposited material films throughout the thruster [6]. Only one new potential failure mode was identified by this test. This failure mode results from material that is sputtered from the cathode-orifice plate and deposited on the upstream side of the cathode keeper electrode. If this sputter-deposited material becomes sufficiently thick, it could flake off and electrically short the cathode to the keeper. The thickest material deposits found anywhere in the thruster were on the upstream side of the cathode keeper. The separation distance between the cathode and the keeper is only 0.51 mm (0.020 inches), a distance that can easily be bridged by a flake of sputter-deposited material.

The data from the 8,000-hr test is being used in the development of models of the engine's principal wear-out failure modes. These models are being used in a probabilistic framework to quantitatively assess the engine failure-risk as a function of propellant throughput (or total impulse) [19 to 24]. This modeling activity is a key part of the NSTAR program to validate the service life of the ion engine.

2.6.1.2 Extended Lifetime Test—After the successful completion of the 8,000-hr test, the last major test in the NSTAR project plan is to demonstrate 150% of the engine-design life using the DS1 flight spare engine (FT2) fabricated by HED. The engine-design life is most easily expressed in terms of the total amount of xenon propellant that the thruster can process. For the NSTAR project, the engine-design life is 83 kg of xenon, which corresponds to 8,000 hours of operation at full power. To demonstrate 150% of the engine life, therefore, requires a test in which 125 kg of xenon is processed by the engine. This test, designated NPT4 in the project plan, was originally designed to follow a representative mission-throttling profile; therefore, some of the test documentation still makes reference to a mission profile test (MPT). The test was later renamed the extended lifetime test (ELT) when it became clear that following a mission profile would not provide as much information about the engine-wearout modes at throttled conditions as a less complicated throttling plan. A secondary objective of this test is to demonstrate extended operation at throttled conditions since the previous project-level life tests had all been performed at the full-power point. It is believed that the full-power point is the most stressing to the engine; however, the ELT is designed to obtain the data necessary to support this assertion.

As of this writing (March, 2000), the ELT has operated FT2 for more than 9,400 hours. The first 500 hours of the test were performed at NSTAR throttle level 12 (TH12). From 500 hours through 5,000 hours, the engine was operated at full power. At 5,000 hours, the thruster was throttled to TH8, which is approximately 63% of full power. The test

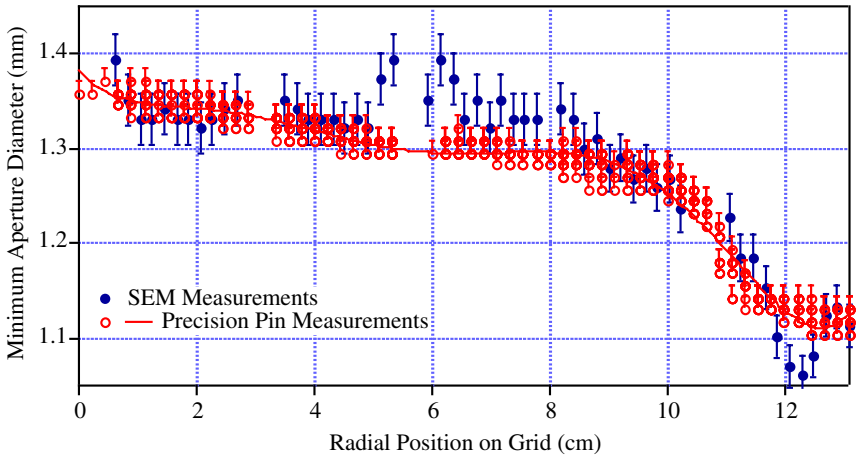

Figure 17. Accelerator Grid Aperture Diameters Measured after the 8,000-hr Test Indicate Significant Enlargement from Their Original 1.14-mm Diameter Values

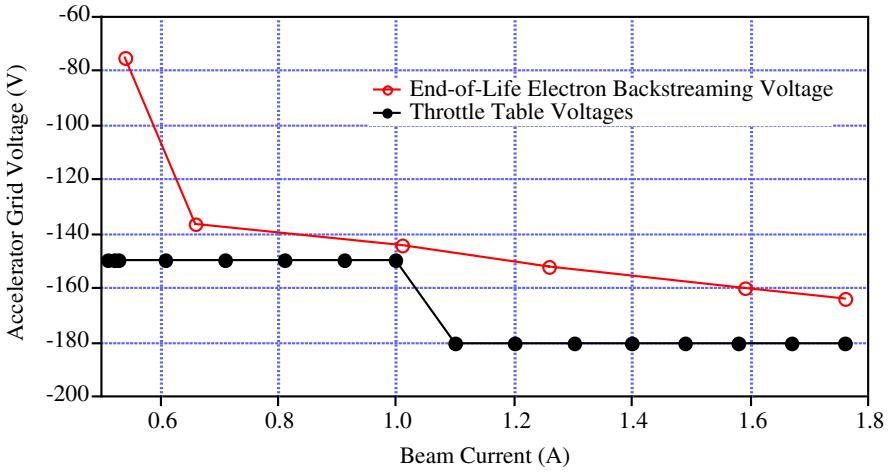

Figure 18. Electron-Backstreaming Voltage Margin at the End of the 8,000-hr Test (EMT2)

plan calls for the thruster to process 30 kg of xenon at this throttle level. The overall efficiency of FT2 over the first 5,400 hours of the ELT is given in Figure 19 for the entire engine-throttling range.

Electron-backstreaming data for FT2 versus run time is compared to that for EMT2 from the 8,000-hr test in Figure 20. The data for FT2 is systematically above that for EMT2 for operation at full power (TH15). This is believed to be a result of separation between the grids of the ion accelerator system being smaller at operating temperature in FT2 than in EMT2. A smaller grid separation requires a more negative accelerator grid to prevent electron backstreaming. The data at TH8 in Figure 20 exhibits a step-function change in the electron-backstreaming limit, even though the beam voltage is the same for both throttle levels. This step-function change is a result of the lower beam-current density for operation at TH8. The higher density of positive ions at full power increases the local space charge between the grids more than at TH8 and, consequently, a more negative accelerator-grid voltage is required to prevent electron-backstreaming at full power.

The purveyance margin for the ion-accelerator system on FT2 is compared in Figure 21 to data taken on EMT2 over the 8,000-hr test. The purveyance limit defines the lower boundary of the engine-throttling envelope as shown in Figure 4 and is qualitatively defined as the beam voltage (for a fixed accelerator-grid voltage and beam current) at which direction impingement on the accelerator grid begins. The purveyance margin is the difference between the purveyance limit and the throttle table-set point for the beam voltage, which is 1100 V at both TH15 and TH8. The purveyance margin data in Figure 1 for FT2 agrees well with that for EMT2 at TH15. The purveyance margin increases at TH15 because of the lower beam current at this throttle level.

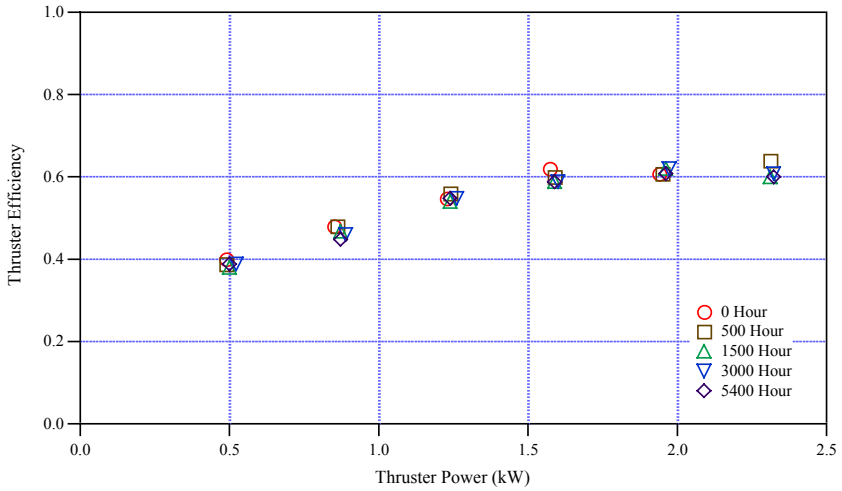

Figure 19. FT2 Efficiency Versus Power during ELT

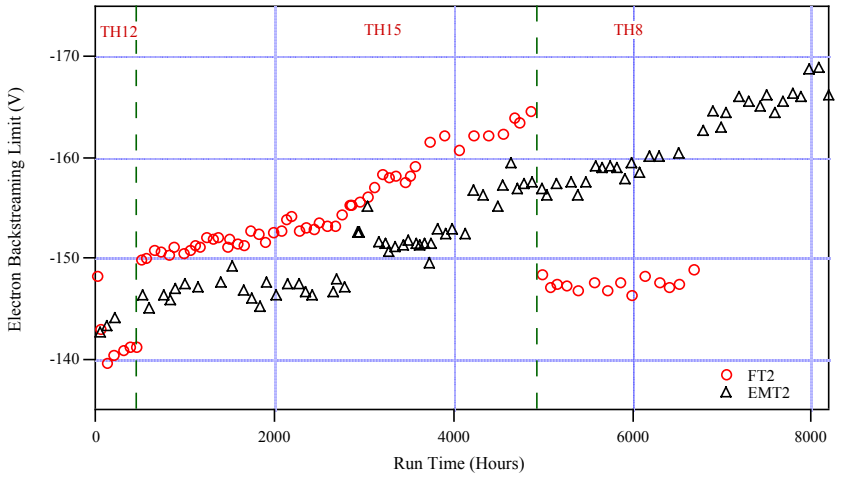

Figure 20. Comparison of Electron-Backstreaming Limits for FT2 and EMT2

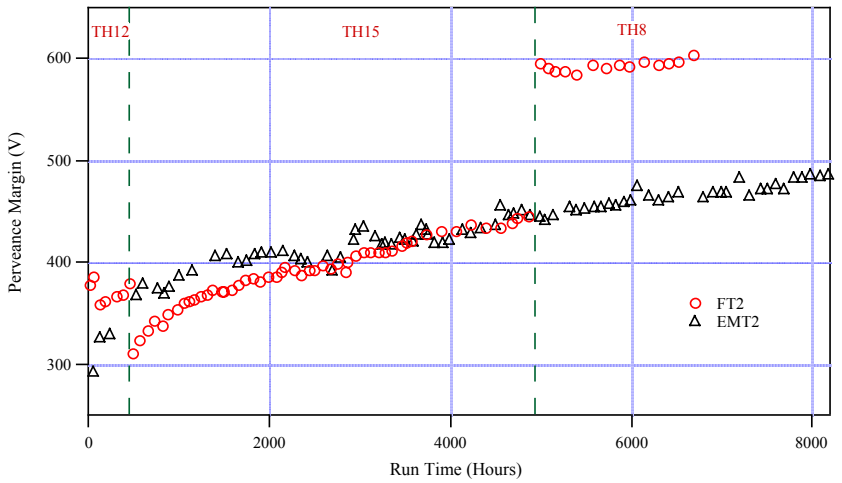

Figure 21. Comparison of the Long-Term Behavior of the Purveyance Margin for FT2 and EMT2

The discharge voltage is a key independent thruster-operating parameter that is used as an indicator of the health of the cathode and strongly affects key thruster-wearout modes. The long-term behavior of the discharge voltage for FT2 is compared to EMT2 in Figure 22. These data indicate excellent agreement for operation at TH15. This good agreement disappeared, as expected, when FT2 was throttled to TH8. Operation at throttled conditions typically results in higher-discharge voltages.

These data and the data given in [25] indicate that the operating behavior of the flight spare ion engine is very similar to that of the engineering-model thruster, EMT2. Since EMT2 exhibited excellent erosion characteristics (i.e., very little erosion), it is anticipated that the flight thrusters will exhibit similar life characteristics. The success of the ELT so far helps verify one of the key assumptions made during the design and fabrication of the flight thrusters: the engine structural and thermal designs could be improved without impacting the engine-service life as long as the critical components (which include the magnetic-field configuration, the cathode and neutralizer, and the ion-accelerator system) were unchanged from the engineering-model thrusters.

2.6.1.3 Characterization Tests—During the time that the 8,000-hr test was being conducted, many questions regarding other details of the thruster operation, behavior of the IPS components at the system level, and interface issues required a series of characterization tests (CTs). A total of 39 CTs were proposed. From this list, 18 of the highest priority tests were selected and executed. Table 9 lists the CTs which were actually performed.

One of the most significant CTs was CT31b, the end-to-end test of key elements of the IPS with the spacecraft power system. This test used an engineering model engine, a breadboard PPU, a breadboard DCIU, a solar-array simulator and the high voltage power conditioning unit (HVPCU) from the spacecraft's power system. This test verified that there were no stability problems associated with handling the large power load represented by the IPS. This test is highly recommended for any future program planning the use of ion propulsion.

2.6.1.4 Engineering Development Tests—To address still further issues associated with the design of the flight engines, another series of tests was developed. This series, called engineering development tests (EDTs), was designed to address primarily structural and thermal issues associated with the engine design. The list of EDTs performed under the NSTAR project is given in Table 10.

2.6.2 Flight Test Program—The validation objectives of the IPS flight test on DS1 include demonstrating the functionality and performance of the system in an environment similar to what will be encountered by future users, the compatibility of the IPS with the spacecraft and science instruments, and autonomous navigation and control of the IPS with minimum ground-mission-operations support.

2.6.2.1 Operating Modes—The DCIU software is designed to perform the functions described briefly in this section. The system also has a number of fault-recovery functions that are defined in [26]. Only a few of those will be discussed here.

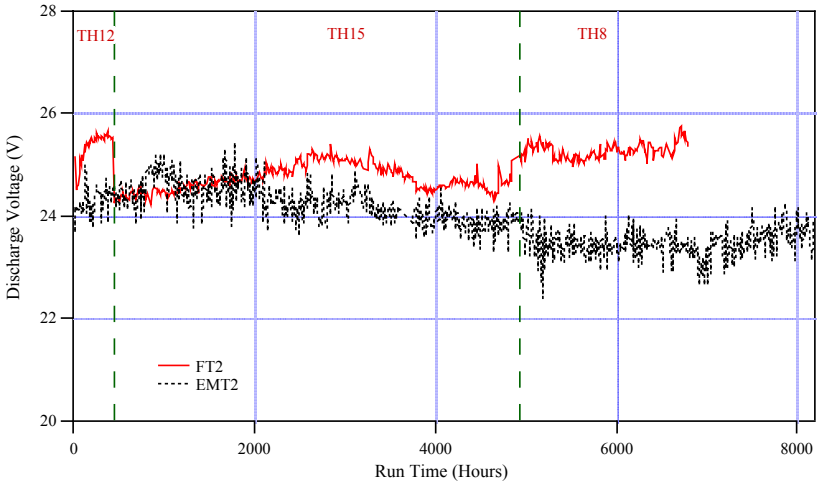

Figure 22. Comparison of the Long-Term Behavior of the Discharge Voltage for FT2 and EMT2

Table 9. NSTAR Characterization Tests

Thruster	Test	Purpose	Description	Duration (hrs)	Location
EMT1b	CT1	plasma screen grounding		1	GRC 5
EMT2	CT19'-1	pre-transport sensitivity	abbreviated TP: only 2 op points	12.2	GRC 5
	CT18	AC frequency components		n/a	JPL148
	CT13	magnetic map	various distances from thruster	n/a	JPL233
	CT19'-2	pre-LDT sensitivity		~5	JPL148
EMT3	CT5	low flow start–3 sccm		1	GRC 5
	CT6	single plena		6	GRC 5
	CT14	empirical thermal measmts	part of EDT2b	9	GRC 5
	CT22b	measure PPU in power quality	BBPPU during recycle	~8	JPL148
	CT27b	PPU input impedance		2	GRC 5
EMT4	CT31b	system end-to-end power stability	includes HVPCU	~25	JPL149
	CT36b	SAS IF verification		~16	JPL149
	CT36c	diode mode trial		1	JPL149
SPOT	CT31b	system end-to-end power stability	includes HVPCU	n/a	JPL149
n/a	CT33	DCIU-XEM1 c/o		n/a	JPL233
SPOT	CT22a	same as CT22b	BBPPU during recycle	n/a	JPL148
SPOT	CT24	PPU start circuit	effects on DS1	n/a	GRC 5
SPOT	CT27a	PPU input impedance		n/a	GRC 5

Cathode Conditioning—After launch, the cathodes are heated for several hours to help drive off oxidizing impurities from the inserts. This sequence is initiated by a single command and controlled by the DCIU.

Thruster Ignition—This operating mode begins with pressurizing the plenum tanks to the proper values, starting propellant flow to the engine, and preheating the cathodes prior to ignition of the neutralizer discharge. After 210 seconds of heating, the neutralizer high-voltage-pulse ignitor is started. After neutralizer-keeper current is detected, the heater and ignitors are turned off and the discharge is ignited. When both discharges have successfully lit, the high voltage is turned on at the minimum power level and the engine is throttled to the final setpoint. The accelerator-grid voltage is set to –250 V for two hours after ignition, then is increased to the correct throttle-point value.

Steady State Operation—The DCIU is capable of operating the thruster at any one of 16 discrete throttle levels from a throttling table stored in memory. This table contains the setpoints for the PPU power supplies and the XFS pressures and can be modified by ground command. The NSTAR 16-level-throttle table showing the entire range of operation is listed in Table 11. The DCIU commands the PPU power supplies to deliver these values and controls the XFS valves to maintain the desired pressures in steady-state operation. The beam-current setpoint is maintained by closed-loop control of the discharge current.

Throttling—When a new throttle level is commanded, the DCIU ramps the XFS pressures and the PPU outputs to the new values. If the power level is being increased, the flows are raised before the engine power is changed. To throttle down, the electrical parameters are changed first, then the flow rates.

Thruster Power Down—In this operating mode the power supplies are turned off and all XFS valves are closed.

Continuous Recycling Fault Mode—The DCIU monitors the number of recycle events initiated by the PPU under high-voltage fault conditions. If 25 or more are recorded in a 90-second time period, the engine is shut off and a fault flag is set.

Grid Clear Fault Recovery—In the event of a physical short between the grids that cannot be cleared by recycling or mechanical methods, the DCIU can be commanded to execute a grid-clear operation. In this operating mode, internal relays in the PPU are closed to apply the discharge supply to the ion optics. The supply is then turned on at a pre-determined current level for a specified period of time in an attempt to resistively heat and to vaporize the short.

These DCIU functions can be called with ground commands. In addition, the spacecraft can generate commands to the IPS to perform certain operations. The IPS is throttled autonomously by the spacecraft to track the solar-array output. DS1 also includes an autonomous system (AutoNav) to navigate the spacecraft to the next encounter target. This system contains an optimized trajectory that was computed on the ground and a catalog of ephemerides for a number of stars, asteroids, planets, and DS1 target bodies.

Table 10. NSTAR Engineering Development Tests

Test	Purpose	Description	Thruster	Duration (hrs)	Location
EDT1a	initial vibe		EMT1b	n/a	NTS
EDT1b	follow-up vibe	with 3rd mounting pt	EMT1c	n/a	NTS
EDT1c	TGA vibe @ .2 g2/Hz	practice for FT#1	EMT1d	n/a	JPL144
EDT2a	cold start, etc.	downstream open	EMT3a	29	GRC 5
EDT2b	2nd phase thermal	+ downstream cover	EMT3a	65	GRC 5
EDT2c	3rd phase thermal	+ gimbal sim plate	EMT3b	334	GRC 5
EDT2d	4th thermal	+ DS1 thermal shield	EMT4	20	GRC 5
EDT2e	final thermal	same as 2d	PFT	41	GRC 5
EDT5	thrust stand performance	w/ modified ExB	EMT3	28	GRC 5
EDT6	500 hr cathode erosion		EMT3	500	GRC
EDT7a	Internal B field		EMT3	n/a	GRC
EDT9	mesh separation		EMT4	8	GRC
EDT12	screen grid saturation		EMT3	4	GRC
EDT16a	shorted discharge keeper		EMT3	3	GRC
EDT20a	plume tests		EMT3	12	GRC

Table 11. Flight Throttle Table of Parameters Controlled by the DCIU

NSTAR Throttle Level	Mission Throttle Level	Beam Supply Voltage (V)	Beam Supply Current (A)	Accelerator Grid Voltage (V)	Neutralizer Keeper Current (A)	Main Plenum Pressure (psia)	Cathode Plenum Pressure (psia)
15	111	1100	1.76	–180	1.5	87.55	50.21
14	104	1100	1.67	–180	1.5	84.72	47.50
13	97	1100	1.58	–180	1.5	81.85	45.18
12	90	1100	1.49	–180	1.5	79.29	43.80
11	83	1100	1.40	–180	1.5	76.06	42.38
10	76	1100	1.30	–180	1.5	72.90	41.03
9	69	1100	1.20	–180	1.5	69.80	40.26
8	62	1100	1.10	–180	1.5	65.75	40.26
7	55	1100	1.00	–150	2.0	61.70	40.26
6	48	1100	0.91	–150	2.0	57.31	40.26
5	41	1100	0.81	–150	2.0	52.86	40.26
4	34	1100	0.71	–150	2.0	48.08	40.26
3	27	1100	0.61	–150	2.0	43.18	40.26
2	20	1100	0.52	–150	2.0	39.22	40.26
1	13	850	0.53	–150	2.0	39.41	40.26
0	6	650	0.51	–150	2.0	40.01	40.26

Periodically (one-to-three times per week) during a burn, the system automatically turns the spacecraft to optically observe the positions of a number of these bodies against the stellar background and calculates the spacecraft position. The heliocentric orbit is then determined and the trajectory propagated to the next target. Required course changes are generated by the maneuver design element and accomplished by varying the IPS-thrust direction and duration. When enabled, this technology dramatically reduces the need for mission operations support, as described below.

2.6.2.2 The NSTAR Throttle Table—The NSTAR 16-point throttle table contains the IPS setpoints required to operate the system over a chosen throttling range. A corresponding mission-throttle table containing the flow rates, thrust, and PPU input- and output-power levels is maintained in spacecraft memory to enable the mission-trajectory calculations performed by the Nav Manager. The complete NSTAR mission table is shown in Table 4. The development of these throttle tables is described in this section.

Power throttling is accomplished by varying the beam voltage and current. The engine-throttling envelope with

lines of constant-beam power is shown in. The boundaries of this envelope represent the maximum beam voltage and current capabilities, the minimum-beam current (which is determined primarily by the minimum-discharge current) and the beam-voltage-purveyance limit. The NSTAR throttle table was designed to maximize the specific impulse; therefore, the power is varied with the beam's current throttling over most of the range. The lowest-power levels are achieved by operating at the minimum beam current and throttling the beam voltage.

The discharge-chamber-flow rate was selected to give the propellant utilization shown in Figure 23. The propellant efficiency of 0.9 was selected at high power levels as a compromise between maximizing total engine efficiency and minimizing double ion production, which can drive internal-erosion rates. A propellant efficiency of 0.90 to 0.91 is maintained over most of the range. At the lowest powers, the double-to-single ion-current ratio is low; therefore, the propellant efficiency was chosen to give a discharge loss that yielded the correct total power at that point.

The thrust in the mission-throttle table is calculated from the engine's electrical setpoints,

$$T = \alpha F_t J_b \left(V_S - V_g \right)^{1/2} \left(\frac{2M}{e} \right)^{1/2} \qquad (1)$$

where J_b is the beam current, V_S is the beam power-supply voltage, V_g is the coupling voltage between neutralizer common and the facility ground or ambient-space plasma, M is the mass of a xenon ion, and e is the charge of an electron. The factors α and F_t correct for the doubly-charged ion content of the beam and thrust loss due to non-axial ion velocities [5]. A constant value of 0.98 for F_t based on earlier 30-cm thruster ground tests and a value of α based on a curve fit to centerline double ion-current measurements as a function of propellant utilization efficiency in a 30-cm, ring-cusp inert-gas thruster [27] were used. Earlier direct measurements of thrust from the LDT agreed well with the calculated value [5,6]. More recent measurements with the flight thrusters were somewhat lower than the calculated values for intermediate throttle levels. The difference between the measured thrust and the table values is shown in Figure 24.

The power required for a given thrust level increases over the engine lifetime due to wear [5,6]; therefore, two tables representing beginning-of-life (BOL) and end-of-life (EOL) were developed. These have the same engine setpoints shown in Table 11 but different engine-power levels. The BOL table was developed primarily through testing with engineering-model thrusters and updated with data from pre-flight measurements with FT1. The EOL table was based largely on measurements from the 8200-hour test of EMT2. The power at the lowest throttle levels was extrapolated from performance curves obtained after about 6500 hours of operation. The extrapolations were based on sensitivity data, which were used to correct for slight differences in some of the controlled parameters. The difference between BOL- and EOL-engine power is plotted in Figure 25. Additional measurements taken at some of these throttle levels after about 6900 hours of operation in the LDT are also shown. They suggest that the EOL power at some of the lower throttle levels is overestimated in the throttling table. BOL data obtained with the two flight thrusters demonstrates that their initial performance agrees well with the table values.

The PPU input power corresponding to a given engine power is determined by the PPU efficiency. The flight-PPU efficiency of was characterized as a function of input-bus

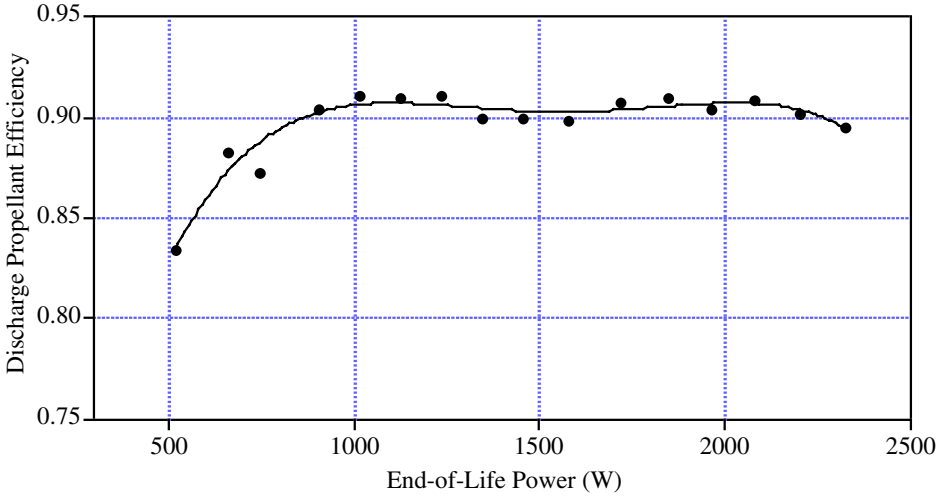

Figure 23. NSTAR Ion-Thruster Discharge-Propellant Utilization Efficiency

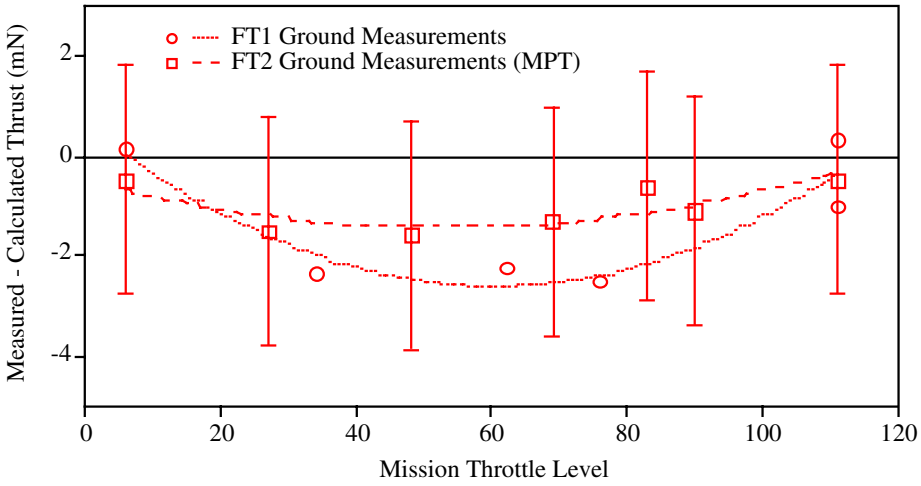

Figure 24. The Difference Between Measured and Calculated Thrust over the NSTAR Throttle Range

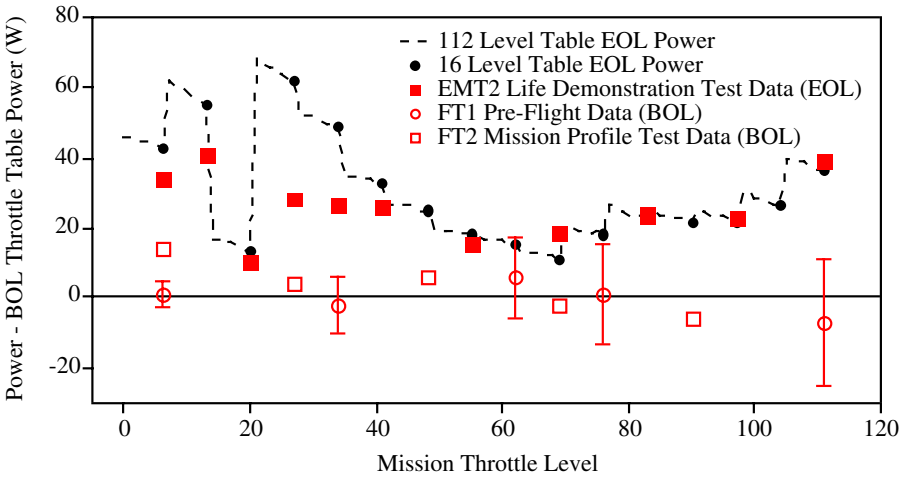

Figure 25. Difference Between a Given Power Level and the Beginning-of-Life Power

voltage and temperature in several ground tests, as shown in Figure 26. The lowest measured values over this range of parameters were used to define the lowermost line in the figure. This conservative estimate of PPU efficiency was used to generate the PPU input powers in the throttle table.

In order to make finer steps in power throttling to more closely track the solar-array peak power, a 112-point throttle table was also developed for use in flight. Power throttling between the 16 NSTAR throttle points is accomplished by varying the beam voltage to give steps that are approximately 20 W apart. A 16-point subset of this table is loaded into the DCIU to provide fine throttle control over a restricted power range for a given mission phase.

2.6.2.3 Post-Launch IPS Operation and Validation Activities—Operation of the ion propulsion system during the DS1 primary mission can be organized into several phases, which are summarized in this section.

Decontamination—The first IPS in-space activity was a bakeout of the downstream portion of the propellant-feed system that occurred six days after launch. Prior to this, the thruster axis was oriented 90° away from the Sun and the thruster front-mask temperature was –45° C. The spacecraft was turned so that the angle between the axis and the Sun was 30° to warm the thruster and feed system. Over a 29-hour period the thruster temperature exceeded 110° C and the XFS lines reached more than 45° C. This was done to help remove any residual contaminants in the portions of the feed system that had been exposed to air prior to launch. The cathode-conditioning sequence was then executed to bakeout the cathode inserts. Finally, 16 days after launch, the discharges were operated for four hours at high power levels to further bakeout the engine prior to application of high voltage.

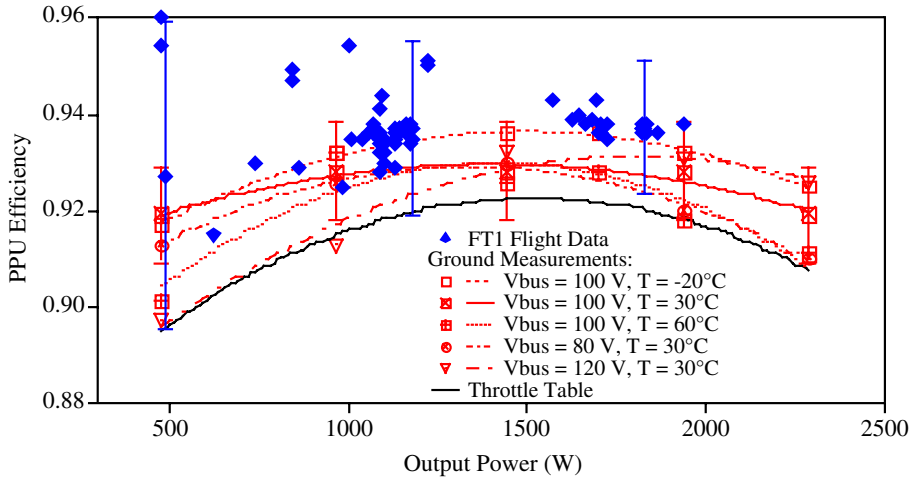

Figure 26. In-Flight Measurements of PPU Efficiency Compared to Ground Test Data

Initial Start and Grid Short—The following day the first engine ignition occurred. Both cathodes lit properly and the engine ran nominally at the minimum-power point for 4.5 minutes before continuous recycling caused a thruster shutdown. A short between the grids was suspected, but at this point a failure of one of the high-voltage supplies could not be ruled out. Fourteen additional start attempts were made under various engine-thermal conditions (created by spacecraft turns toward or away from the Sun); all ended in continuous recycling when the high voltage was applied.

Troubleshooting—Taking advantage of the flexibility of the thrusting start date, a detailed investigation of the problem was undertaken. Several options were identified, including: attempting a grid-clear command, thermally cycling the engine to force a mechanical separation of the grids that might dislodge a particle, running additional recycles, and developing additional diagnostics to help identify the fault.

The NSTAR PPU is designed to deliver 4 A into a grid short to clear those that are not cleared by recycles. However, this system was designed primarily to clear thin molybdenum flakes generated by spalling of sputter-deposited films inside the discharge chamber after many thousands of hours of operation. Grid shorting this early in a mission was more likely due to particulates from the launch-vehicle payload fairing or generated during the payload preparation, which could be much larger than films from the discharge chamber. The risk of permanently welding a large particulate between the grids with the standard-grid clear circuit was not known, so an experimental and theoretical effort to characterize the grid-clear process was undertaken prior to using it under these circumstances. The results of this investigation are reported in [28].

Thermal and structural models of the ion optics were also coupled during this period to determine the mechanical effect of thermally cycling the grids. This modeling showed that significant transient changes in the grid spacing can be achieved by turning the spacecraft to heat or cool the grids. This technique was used to clear grid shorts on the SERT II flight experiment [29] and appeared to have a very minimal risk. During the two-week problem-investigation period, the spacecraft was turned several times; this thermally cycled the grids over greater than a 100° C range.

The IPS is designed with hardware interlocks that prevent operation of the high-voltage supplies before the discharges are ignited; therefore, it was not possible to command these supplies to turn on separately to test them. The DCIU software was modified to provide brief bursts of high-speed data for various PPU electrical parameters during recycles to help diagnose which supplies were affected. Finally, a test involving operation of the discharge supply only, with no propellant flows (which is allowed by the system), was developed. If the grids are shorted, the accelerator-grid-voltage telemetry will change when the discharge-open-circuit voltage is applied; otherwise it remains close to zero. This is a clear discriminator between open circuits and shorts on the ion optics.

Recovery Start—Thirty-one days after launch, the discharge-only test was executed; the results suggested that the grids were not shorted. Another start attempt was then made, primarily with the intent to gather high-speed engine data during continuous recycling to help diagnose the fault. Fortunately, the engine started properly this time and has continued to run flawlessly since this point. Apparently, the thermal cycling successfully cleared debris lodged between the grids.

The origin of the surmised debris cannot be conclusively identified, but the event itself points to the importance of contamination control on the engine pre-launch. Much care was taken to launch with a dust- and debris-free thruster, in both design and handling. An especially concentrated effort

was devoted to the nearby solid rocket motor (SRM) dome surfaces and the spacecraft-separation system, with design changes actually implemented once the contamination analysis identified possible sources for debris in the original plan.

In the future, all reasonable origins for debris should be studied and identified and appropriate protection should be implemented.

First Performance Test—Over the next 335 hours, the engine was operated at power levels ranging from 0.48 to 1.94 kW to characterize the BOL performance. This burn was used to contribute to the required spacecraft ΔV, but was not controlled by AutoNav. The throttle levels were dictated primarily by the validation objectives. This test was designated IPS Acceptance Test 1 (IAT1).

Deterministic Thrusting—IAT1 was followed by 95 hours of thrusting at power levels ranging from 1.7 to 1.86 kW. These initial operations also contributed to the required total impulse, but were executed with ground commands. These were followed by a coast period of 74 days and seven navigational burns (NBURNs) totaling 912 hours of operation. These maneuvers were executed autonomously by AutoNav and used automatic-peak-power tracking to determine the maximum achievable throttle level. The first of these, NBURN 0, did not use the optical navigation for spacecraft-position determination; however, all subsequent NBURNs have exercised the full AutoNav capability. This part of the mission is on an outbound portion of the trajectory, so the available array power decreased continuously. NBURN 0 was run with engine power levels ranging from 1.73 to 1.62 kW, while the following six NBURNs were performed with power levels of 1.18 to 0.71 kW. These burns completed the deterministic thrusting required for the encounter with asteroid Braille.

Second Performance Test—After another coast period of 21 days, a second throttling test was performed. This brief test, designated IAT2, was restricted to power levels ranging from 0.49 to 0.98 kW by total solar-array power.

2.6.2.4 In-Flight System Performance—One of the primary objectives of the flight-validation activity is to verify that the system performs in space as it does on the ground. The parameters of interest to future mission planners are those in the mission-throttle table: thrust and mass flow rate as a function of PPU input power. In this section, the system power, thrust, and mass-flow-rate behavior will be evaluated in terms of the throttle table.

PPU Power Input Requirements—The PPU input power is determined by the PPU output power (engine-power requirement) and the PPU efficiency. The difference between the in-flight engine, input power and the BOL throttle-table power is shown in Figure 25. These power values are based on the individual power-supply current and voltage-telemetry readings. The total engine power consumed during the IAT1 throttle test and initial operations differed from the table values by only about 2 W on average, although the uncertainties are much larger than this, as shown by representative error bars on the figure. The engine-power requirement increased by 12 to 15 W with time, however, as the data from NBURNs 1 to 3 and IAT2 show. This is a normal consequence of engine aging [5,6], and the total power at this point in the mission is still less than the EOL power used in the throttle table, which is represented by the solid line in Figure 25. This increased power demand is due primarily to increased discharge-power losses, as discussed in the next section.

In-flight measurements of the PPU efficiency suggest that it is higher than that measured in ground tests, as shown in Figure 26. These values are based on the total engine power and PPU high-voltage bus current and voltage telemetry with an additional 15 W assumed for the low voltage-bus-input power. There is no telemetry for the low voltage bus; however, ground testing showed a 15 W loss for all conditions. The efficiency is sensitive to the line voltage and the temperature, as the ground data show. The in-flight measurements were taken with line voltages of 95 ±5 V and baseplate temperatures ranging from 0 to 37° C, so they should be compared with the solid line in the center of the preflight data and the highest dashed line. The range of uncertainty in these measurements encompasses the ground test data; however, the in-space measurements appear to be higher systematically by about one percentage point. This apparent performance gain is not understood and may be due to a systematic error in the ground or flight measurements.

If the PPU efficiency is actually higher than anticipated, it more than offsets the increased output-power requirements observed so far in the primary mission. Figure 27 displays the difference between the observed PPU-input power and the BOL–input power from the throttle table. The input power required early in the mission was approximately 20 W lower than expected because of the higher PPU efficiency. The data from the NBURNs and IAT2 show that the input power is just now approaching the BOL throttle-table value.

IPS Thrust—The acceleration of the spacecraft is measured most accurately from changes in the Doppler shift of the telecommunications signals. With models of the spacecraft mass as a function of time, the Doppler residual data can be used to measure the thrust of the IPS with an uncertainty of less than 0.5 mN. Preliminary thrust measurements have been obtained so far from IAT1, the initial operations, and NBURN 0. The flight-beam voltage and current values, which determine to a large extent what the thrust is, are

slightly different from the setpoints in the table. The flight-thrust measurements are, therefore, compared to the thrust calculated from the actual electrical parameters rather than the table values. The difference in the measured and calculated thrust is shown in Figure 28, with the curve fits to similar data obtained with a thrust balance in ground tests. The ground and flight data agree well with the calculated values at low power levels, but are lower at intermediate powers. The flight data suggest that the difference in true thrust and calculated thrust grows linearly with power, peaking at 1.6 mN lower than expected at mission level 83 (1.82 kW engine power). The error bars shown in this figure are based on the uncertainty in the measured thrust and do not include errors in the calculated thrust.

This discrepancy may also be due to a systematic error in the flight telemetry, although the agreement with ground data argues against that conclusion. As Equation (1) shows, the true thrust might be lower than calculated because of a higher double-ion content, greater beam divergence than observed in the previous 30-cm thruster tests, or differences in the coupling voltage in space compared to ground tests. Additional measurements and analysis will be required to resolve this issue.

Although the actual thrust appears to be slightly lower than expected, at the beginning of the mission the overall system performance was still very close to the BOL throttle-table

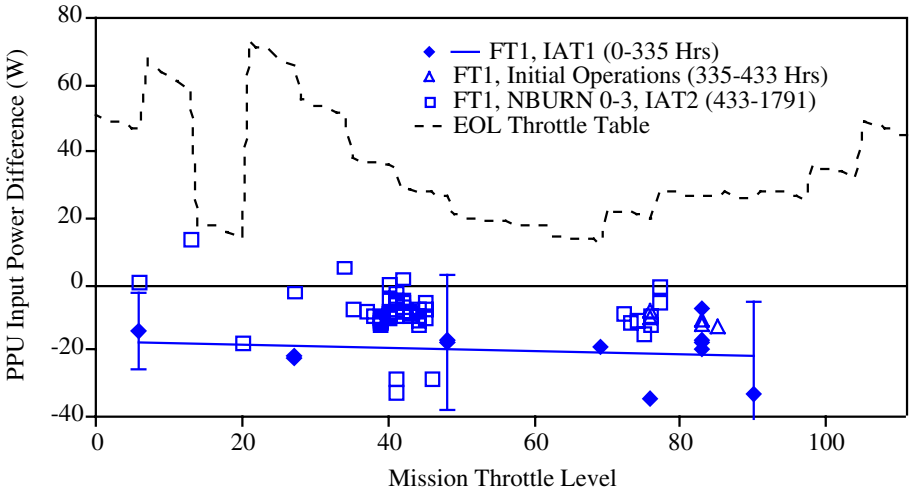

Figure 27. Difference Between a Given Input Power to the Flight PPU on DS1 and the Corresponding Throttle Table BOL Value

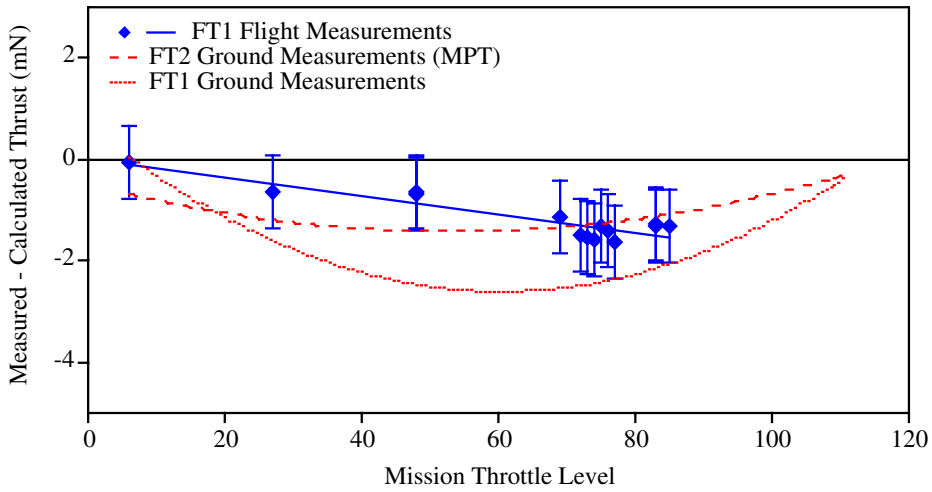

Figure 28. Difference Between Measured and Calculated Thrust in Flight Compared to Ground Measurements

level in terms of thrust for a given PPU input power. Figure 29 shows that at the beginning of the mission the higher PPU efficiency largely compensated for the lower thrust. In this comparison, the thrust is within 0.5 mN of the table values. The gap between the two widens as the engine wears and the total engine-power requirement for a given throttle level grows. The PPU input power required for the thrust levels measured during NBURN 0 has exceeded the EOL throttle-table power for an equivalent thrust.

The thrust-vector behavior in-flight is similar to that observed in ground tests. The engine is mounted on a two-axis gimbal with range of ±5°. When the IPS is not operating, a hydrazine attitude-control system is used for 3-axis stabilization. After ignition of the ion thruster, control in two axes is transferred to the IPS gimbal system. Potentiometers on each axis of the gimbal provide a measure of the thrust-vector stability during IPS operation. There is a brief transient after transfer of control; however, after that the mean value of the gimbal angle appears to be stable over long periods of time. The thrust vector of the flight engine relative to the thruster axis was measured using a thrust-vector probe [16] prior to integration and alignment on the spacecraft. The gimbal-angle data in Figure 30 show that this alignment was excellent. They also demonstrate that the thrust vector changes slightly with throttle level, as shown in previous ground tests [16].

Propellant Flow Rates—The performance of the xenon feed system is discussed in detail in [9]. In general, the performance has been excellent, although the flow rates are slightly higher than the throttle-table values. The mean value of the main flow is 0.05 to 0.14 sccm (about 0.4 to 1.0 percent) high, while that of the two cathode flows is 0.03 sccm (about 1.0 percent) high. This is in part intentional. As Figure 31 shows, the XFS bang-bang regulators result in a sawtooth-pressure profile. The control system is designed so that the minimum pressure in this sawtooth yields the throttle table flow-rate values. In addition to this deliberate conservatism, there is a slight bias in both regulators because one of each of the three pressure transducers on the two plena had a slight offset after launch.

Overall System Performance—The propulsion system performance can be summarized in terms of specific impulse and efficiency. At the beginning of the mission, the Isp was about 60 seconds lower than expected and the engine efficiency was 2 to 2.5 percentage points lower than the throttle-table values. The measured performance was still excellent, with a measured efficiency of 0.42 to 0.60 at Isps ranging from 1960 to 3125 seconds over an engine-throttling range of 478 to 1935 W. Measured mission-planning performance parameters are listed in Table 12.

2.6.2.5 Engine Behavior In-Flight—The engine behavior in space has been very similar to that observed in ground testing. The detailed operating characteristics of the engine are discussed in this section.

Engine Ignitions—A total of 32 successful engine ignitions have occurred in the first 1791 hours of the primary mission with only one failure to achieve beam extraction (due to the initial grid short discussed above). The data from the first 25 ignitions are reviewed here. The nominal heater-current value is 8.5 A; the actual cathode and neutralizer-heater currents in flight have been constant at 8.444 A and 8.375 A, respectively. The time history of the heater voltages, which are an indicator of heater health, are plotted in Figure 32. The uncertainty in these measurements is about 12%. The first 15 ignitions include the first successful engine start

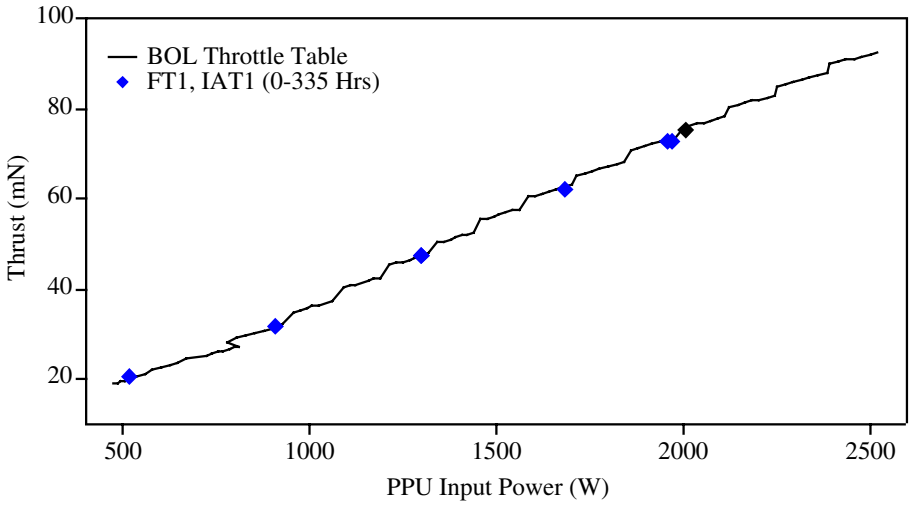

Figure 29. Thrust Measured in Flight as a Function of PPU Input Power Compared to the Throttle Table Values

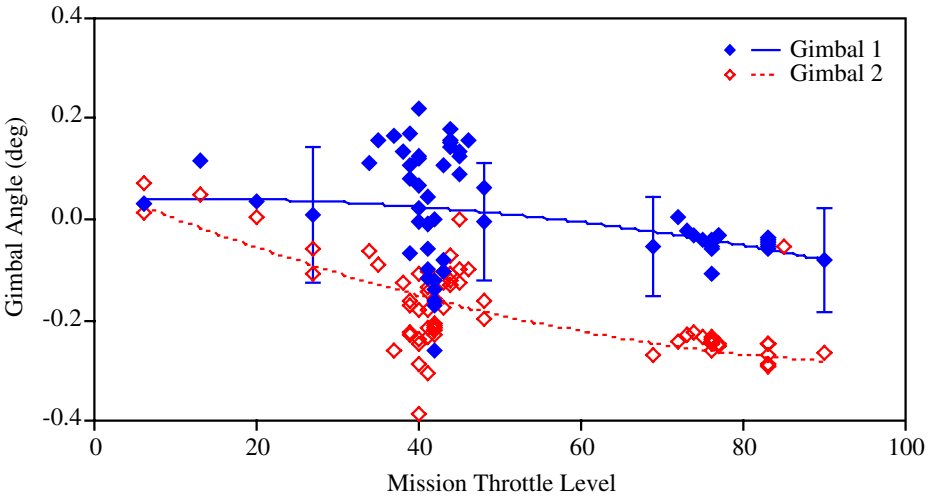

Figure 30. In-Flight Gimbal Positions as a Function of Mission Throttle Level

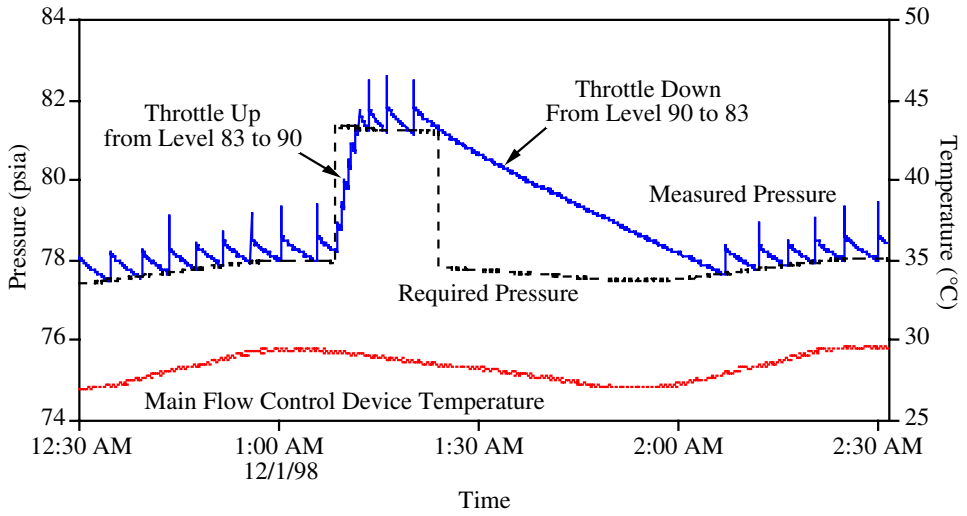

Figure 31. Example of Flow Rate Throttling

and 14 start attempts after continuous recycling shut the thruster off. The peak-heater voltage is a function of the heater impedance, current, and temperature. The data show that the heater voltage increases in any rapid sequence of ignitions because the conductor is hotter at the beginning of each consecutive start. The subsequent data show that the heater voltage is also higher when the initial thruster temperature (indicated by the front-mask temperature in the plot) is higher. The scatter in the peak voltages under similar temperature conditions is low and very similar to that observed in ground tests.

The time required for the cathodes to ignite after the 210 seconds heat phase and application of the high voltage-ignitor pulses is plotted in Figure 33. The neutralizer ignition delays show trends that also follow initial temperature, with 20 to 80 second delays observed for the lowest temperatures. Delays of up to 86 seconds were also observed during ground-thermal tests at the lowest temperatures [13] and are not considered to be a concern. In all cases, the discharge cathode has ignited 5 to 6 seconds after successful neutralizer ignition, which reflects delays in the start sequence. Its ignition reliability may be higher because it has a slightly higher heater current and because it automatically goes through a longer heat phase when the neutralizer ignition is delayed.

Throttling Characteristics—The throttling sequences were in all cases executed properly by the DCIU after receiving ground commands. An example of the throttling sequence is shown in Figure 31 and Figure 34. The IPS Manager software onboard the spacecraft is also designed to

Table 12. Flight Engine Performance Measured in Space

NSTAR Throttle Level	Mission Throttle Level	PPU Input Power (kW)	Engine Input Power (kW)	Measured Thrust (mN)	Main Flow Rate (sccm)	Cathode Flow Rate (sccm)	Neutralizer Flow Rate (sccm)	Specific Impulse (s)	Total Efficiency
12	85	1.99	1.86	75.34	19.99	2.91	2.82	3035	0.602
11	83	1.94	1.82	72.55	18.63	2.75	2.67	3125	0.610
11	83	1.96	1.83	72.63	18.62	2.75	2.67	3131	0.609
10	77	1.84	1.72	69.54	18.59	2.75	2.67	3000	0.594
10	76	1.82	1.70	67.21	17.31	2.58	2.51	3109	0.602
10	75	1.79	1.68	66.81	17.33	2.58	2.51	3087	0.601
10	74	1.77	1.66	66.11	17.33	2.59	2.51	3054	0.595
10	73	1.75	1.65	65.64	17.31	2.59	2.51	3035	0.594
10	72	1.73	1.63	65.15	17.31	2.59	2.51	3012	0.592
9	69	1.67	1.57	62.27	16.08	2.50	2.43	3070	0.597
6	48	1.29	1.22	47.43	11.42	2.50	2.42	3006	0.573
6	48	1.29	1.22	47.39	11.44	2.49	2.42	3004	0.571
3	27	0.89	0.84	31.70	6.93	2.50	2.43	2770	0.511
0	6	0.50	0.48	20.77	6.05	2.50	2.43	1961	0.418

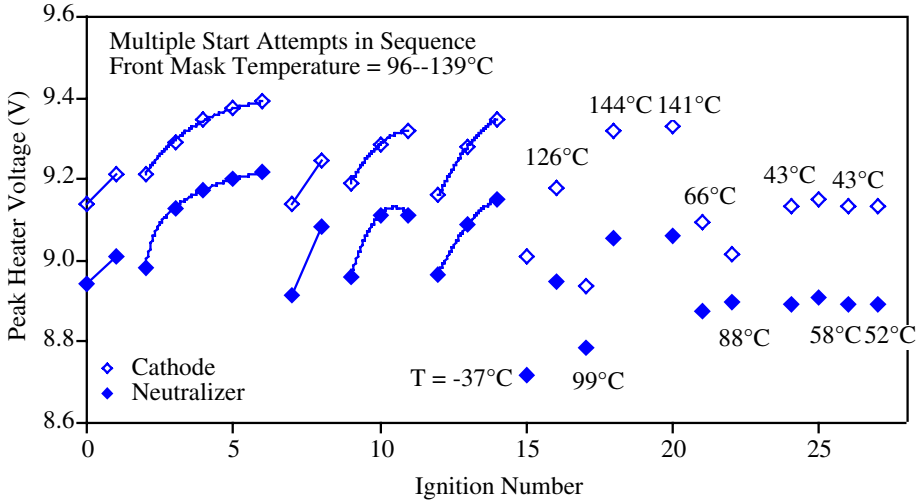

Figure 32. Time History of Peak Cathode and Neutralizer Heater Voltages in Flight

autonomously throttle the engine to track the peak power available from the array. The engine is initially throttled up until auxiliary battery power drain is observed and then decreased until no battery power is required. Anytime battery operation is detected as available array-power drops or the spacecraft's power needs increase, the IPS is commanded to throttle down to accommodate the reduced power. This function was successfully demonstrated in all of the NBURNs, which were accomplished with no ground control required over the detailed engine operations.

Steady-State Setpoint Accuracy—As mentioned above, the flight-flow rates are slightly higher than the throttle-table setpoints. In addition, the beam current is 4 to 13 mA high over a range of 0.51 to 1.49 A. The beam current is controlled in flight to within +2 mA by varying the discharge current in a closed loop. This variation is driven primarily by the flow-rate sawtooth, as shown in Figure 34. The neutralizer-keeper current is 17 mA low at the 2 A setpoint and 10 mA low at 1.5 A. The accelerator-grid voltage is 2 V higher than the setpoint at all operating points. The beam voltage is on average about 3 V lower than the setpoints. The offsets in beam-power supply settings result in slightly higher beam-power levels than the throttling tables assume. This is largely offset by lower neutralizer-power levels, as explained below. All of these parameters are well within the specified flight-system tolerances.

Discharge Performance—As indicated in the previous section, the difference between the total engine power and the throttle-table values is dominated by the discharge-power difference. Discharge performance is summarized in terms of the ion-energy cost (eV/ion) plotted in Figure 35.

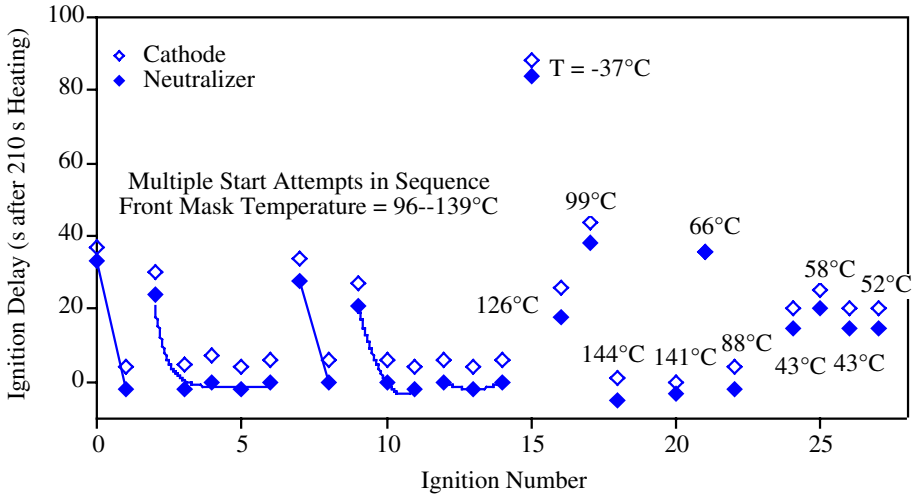

Figure 33. Time History of Cathode and Neutralizer Ignition Delays in Flight

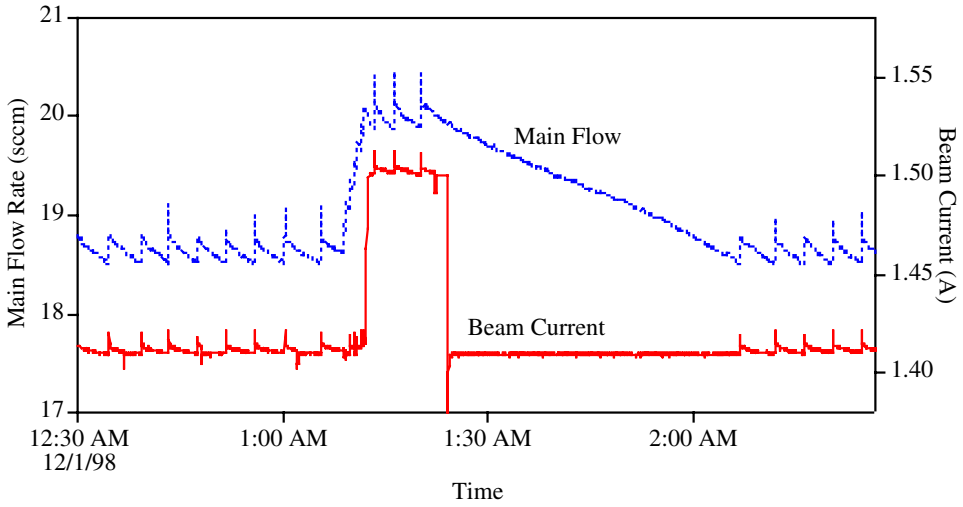

Figure 34. Example of In-Flight Throttle-up and Throttle-down Sequences

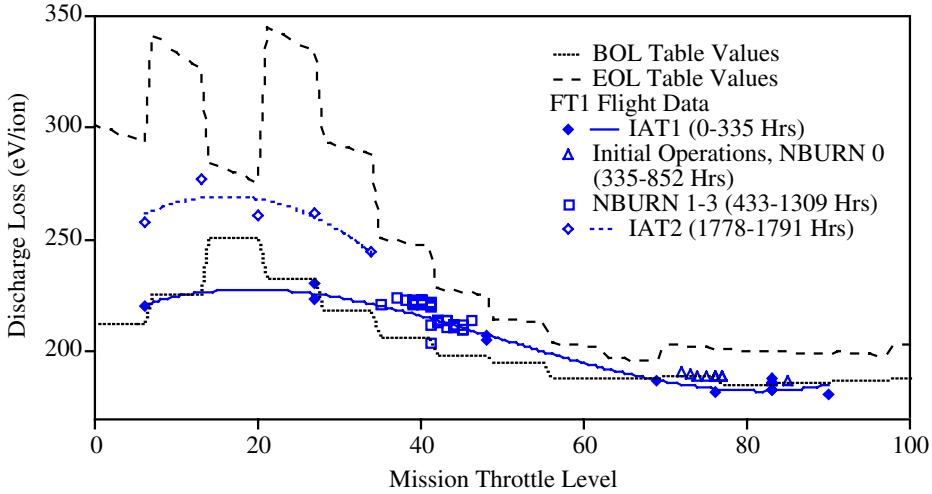

Figure 35. Discharge Loss Measured in Flight Compared to the Throttle Table Values

The standard error of these measurements is 1.5 percent. This plot shows the beginning and end-of-life discharge loss as a function of mission-throttle level. The data from early in the DS1 mission are quite close to the throttle-table values except in the middle of the range (throttle levels 40 to 60), where the flight data are higher. This appeared to be true of the ground measurements as well, suggesting that the BOL throttle-table discharge loss and total power are low by about 10 W in this range. The data from NBURNs 1 to 3 and IAT2 indicate that the discharge losses are increasing with time as a consequence of engine wear [5,6]. The lowest throttle levels are particularly sensitive to engine wear and show the largest increases in flight, up to 40 W. However, all of the data are still bounded by the throttle-table BOL and EOL values.

The discharge voltage and current are compared with the throttle-table values in Figure 36 and Figure 37. The voltages measured in flight are typically within 2% of the throttle-table voltages. The ground-test data are also plotted in this figure and tend to be slightly higher, although some of these measurements have not been corrected for voltage drops in the ground-facility power cables. There is very little drift in the discharge voltage over the course of the flight, which is consistent with long duration ground-test data [5,6]. The discharge current is also close to the BOL table values initially, with the exception of measurements at mission level 48. This is in the range where the table values appear to underestimate true BOL behavior. Unlike the voltage, the discharge current increases with time and drives the discharge power toward the EOL values.

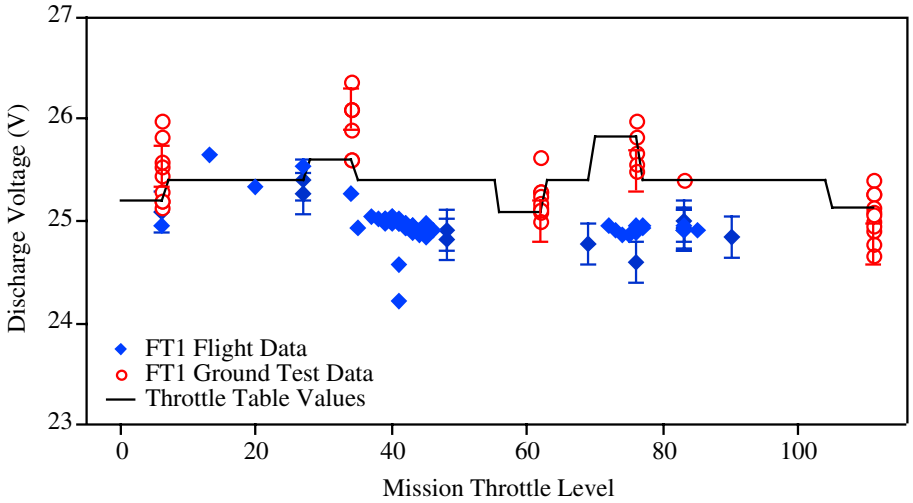

Figure 36. Discharge Voltage Measured in Flight Compared to the Throttle Table Values and Ground Test Measurements

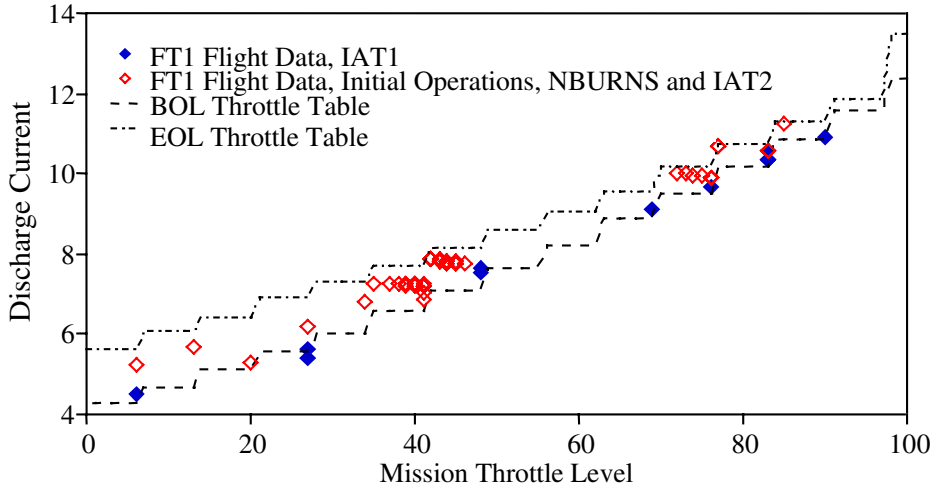

Figure 37. Discharge Current Measured in Flight Compared to the Throttle Table Values

Data on the sensitivity of discharge losses, voltage and current to small variations in flow rates, and beam current from the ongoing extended life test were used to examine the effect of setpoint errors on the flight-discharge parameters. The effects compete and result in negligible changes in these parameters due to the small flow- and beam-current errors.

Ion Optics Performance—The ion optics appear to be performing very well so far in flight. The accelerator-grid-impingement current as a function of beam current is compared to ground-test data in Figure 38. The standard error of these measurements is about 0.03 mA. The data obtained in the ground-test facilities are higher because they include a contribution from charge-exchange reactions with residual tank gas. The flight impingement-current levels in space are about 0.4 mA lower at 0.51 A and 1.7 mA lower at 1.5 A compared to pre-flight measurements in the JPL endurance-test facility, which operates at pressure levels of $2–5\times10^{-4}$ Pa ($1.5–4\times10^{-6}$ Torr) over the full-throttle range. Accelerator grid erosion measurements obtained in long duration tests in this facility are, therefore, conservative. Data obtained in VF5 at NASA GRC, which has a residual-gas pressure about three times lower than that at JPL, show impingement currents that are about 0.4 mA greater than the space values. The ratio of impingement current to beam current is shown as a function of beam current inFigure 39. This parameter, which is used in some probabilistic models of accelerator-grid erosion [19,21,23,24], ranges from 0.17 percent at 0.51 A to 0.28 percent at 1.5 A with a standard deviation of 0.012 percent. A total of 88 high-voltage faults have occurred during 1791 hours of engine operation (excluding those that occurred as a result of the initial grid short). There has been no evidence of electron back-streaming. The discharge loss has consistently increased

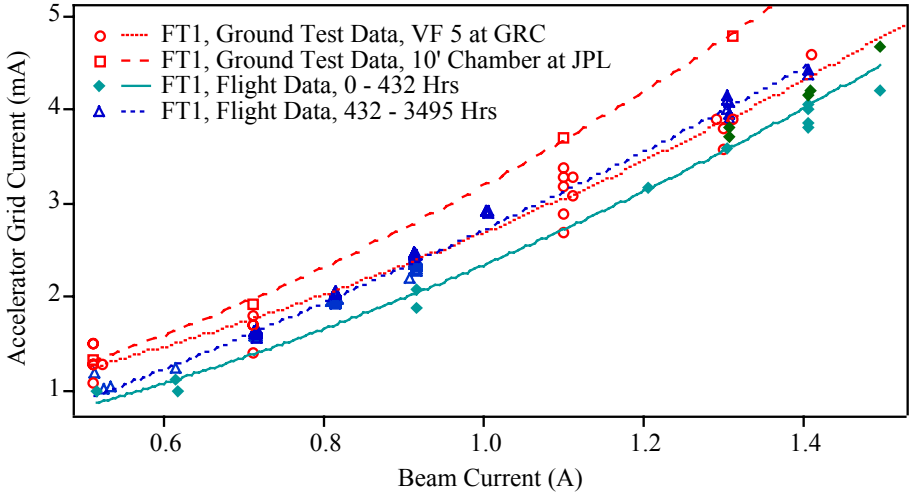

Figure 38. Accelerator Grid Impingement Current Measured in Space Compared to Ground Test Measurements

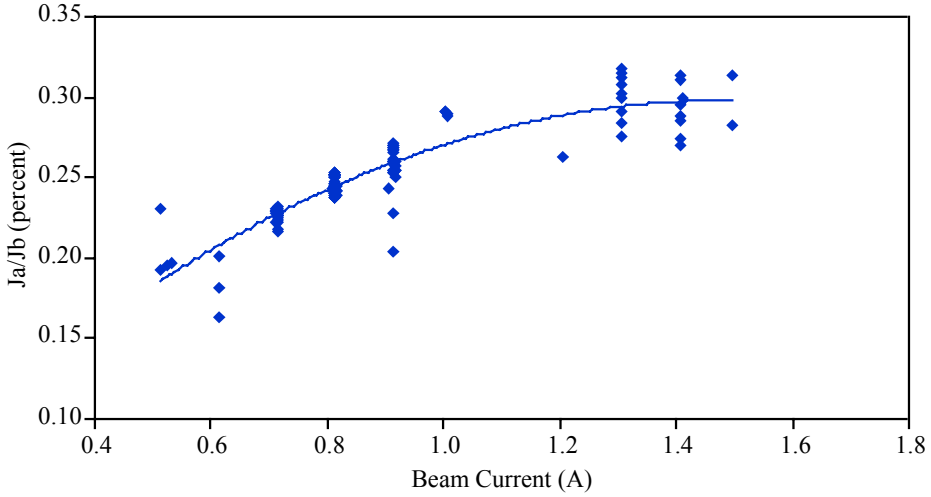

Figure 39. In-Space Ratio of Accelerator Grid Impingement Current to Beam Current

slightly when the accelerator-grid voltage is raised from –250 V after ignition to the throttle setpoint, which is the nominal behavior. This transition is monitored for decreases in the discharge loss, which could signal the loss of electron backstreaming margin.

Neutralizer Performance—The neutralizer-power consumption has been 4 to 7 W lower than the BOL throttle-table values due to a lower neutralizer-keeper voltage, shown in Figure 40. This power savings roughly compensates for a higher beam-power demand due to the beam-current offset. The voltage dropped by about 0.5 V over several days before many of these data were taken in IAT1. The IAT1 data show that at that point in the mission, the keeper voltage was up to 2 V less than the pre-test values. This difference is not yet understood. The voltage has continued to decrease with time, as the data from the initial operations and the NBURNS show. This behavior has been observed in ground tests [5,6] and is an indication of improving emitter-surface conditions.

There is no instrumentation on the DS1 spacecraft that allows the true neutralizer-coupling voltage to be easily determined. The voltage of neutralizer common with respect to the spacecraft ground is metered, and the behavior is shown in Figure 41. To properly compare this with the ground measurements of coupling voltage, also shown in this plot, the spacecraft potential with respect to the ambient plasma must be known. It may be possible to estimate this from the onboard plasma diagnostics; however, this analysis is not yet complete. It is interesting to note that the voltage variation with throttle level has the same slope as that of the coupling voltage in ground measurements and that the magnitude is decreasing with time, which also occurs in ground tests.

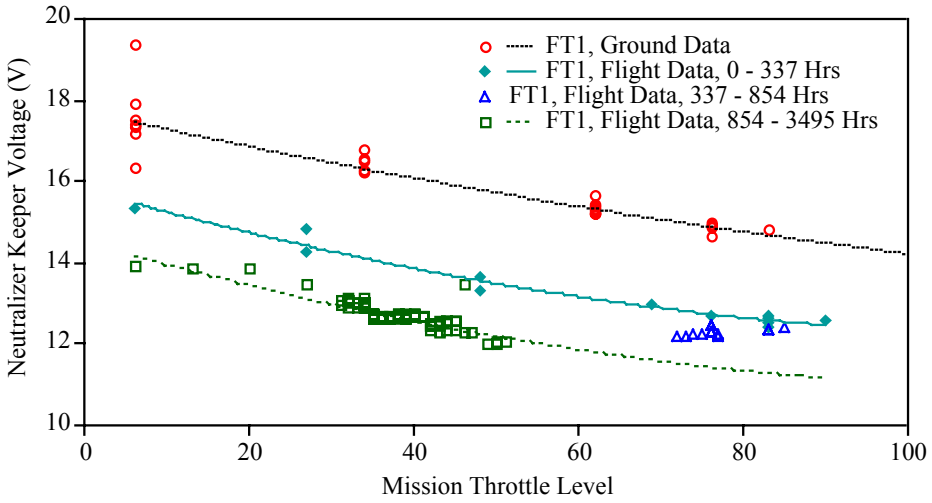

Figure 40. Neutralizer Keeper Voltage Measured in Space and in Ground Tests

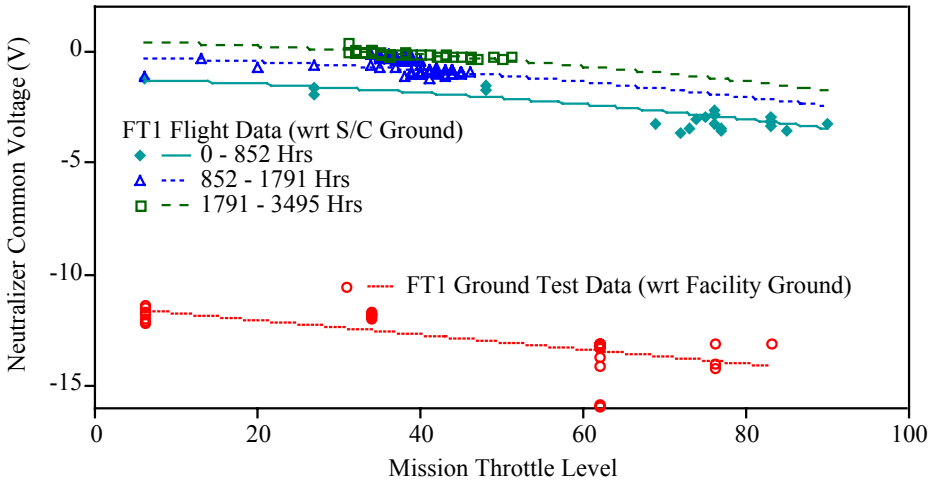

Figure 41. Neutralizer Common Voltage Measured with-Respect-to Spacecraft Ground in Space and with-Respect-to Facility Ground in Ground Tests

2.6.2.6 Mission Operations—Although the total thruster-operating time so far has been orders-of-magnitude longer than that required by impulsive propulsion systems, the mission-operations demands from the IPS have been reasonably minimal (once account is taken for this flight being the first experience with low-thrust navigation and the consequent conservativeness for the sequencing and activity-review processes). Once confidence in the IPS operation was gained, the mission-operations process was as streamlined as originally intended.

This was largely due to the successful implementation of a high degree of spacecraft autonomy. Autonomous navigation has significantly reduced the demands on the navigation- and trajectory-design teams. Spacecraft control of the IPS relieves the ground controllers considerably. In the initial phase of the mission, a number of propulsion engineers were involved in mission operations and validation. However, the final NBURNs have become sufficiently routine at this point that not much workforce is assigned to this area. The flight-data dissemination and analysis has also been largely automated. During Deep Space Network coverage, the spacecraft telemetry is displayed in real time on a Web site that can he accessed by the flight team. Data are also stored in the JPL ground-data system and automatic queries to this system generate files of IPS data periodically that are sent via FTP to all flight team members. A series of macros written in Igor Pro software are used to automatically load, analyze, and plot these data.

The success in reducing mission-operations requirements with automation is an extremely significant result because the fear of excessive operations costs has been a major barrier to the acceptance of ion propulsion for planetary missions. It now appears that the mission-operations costs for SEP-driven spacecraft are similar to those for conventional spacecraft or possibly less in cases where the use of ion propulsion results in shorter trip times.

3.0 Technology Validation Summary

The following key risks were retired by the NSTAR project, and the flight of the ion propulsion system on DS1:

- Adequate engine life—Prior to the NSTAR project, no ion engine intended for primary propulsion had ever been successfully operated for its full design life. The NSTAR project did this and is in the process of demonstrating 150% of the engine design life.
- Guidance, Navigation and Control of an SEP spacecraft—The low-thrust nature of SEP made this a risk area. The operation of the SEP system on DS1 demonstrated that GN&C is not more difficult with an SEP spacecraft, just different.
- Mission-operation costs—Requiring the propulsion system to operate continuously led some to project that a standing army of propulsion and power engineers would be required to operate the spacecraft. However, the electrical nature of SEP lends itself well to autonomous operation, resulting in essentially no significant increase in mission operations cost for SEP vehicles.
- Spacecraft contamination by the SEP system—Slow erosion of the engine results in a non-propellant efflux from the thruster that could contaminate sensitive spacecraft surfaces. Data from DS1 indicates that this efflux travels essentially line-of-sight from the engine and poses no health risk to the spacecraft.
- SEP impacts on science instruments—The charge-exchange plasma generated by the operation of the SEP system is easily detected by onboard plasma instruments. DS1 showed that this low-energy plasma does not interfere with measurements of the much more energetic solar-wind plasma.
- SEP impacts on communication—The charge-exchange plasma generated by the operation of the SEP system could affect the transmission or reception of electromagnetic waves. However, no impact of the SEP system on communications with DS1 could be detected.
- Electromagnetic compatibility (EMC) of the SEP system with the spacecraft—The high-power nature of SEP and the use of strong permanent magnets in the ion engines could make it difficult for the SEP system to be electromagnetically compatible with the spacecraft. DS1 showed that while this issue requires careful engineering, it is an easily tractable problem.

4.0 Future Applications

Many missions have been identified by JPL's advanced mission planning activity as being either enabled or strongly enhanced by the use of solar-electric propulsion based on NSTAR or derivatives of the NSTAR ion-propulsion technology, including: Comet Nucleus Sample Return, Mercury Orbiter, Neptune Orbiter, Titan Explorer, Saturn Ring Observer, Europa Lander, and Venus Sample Return. In addition, it is anticipated that several Discovery Mission proposals will baseline the use of NSTAR-based ion propulsion systems to reduce the cost of going to scientifically interesting but propulsively difficult destinations.

To illustrate the benefits enabled by the use of an NSTAR-derivative SEP system for a Comet Nucleus Sample Return (CNSR) mission, the performce of this mission with SEP for the target-comet 46P/Wirtanen is compared to ESA's chemical-propulsion-based Rosetta mission to the same comet. The Rosetta spacecraft has an initial wet mass of 2,900 kg and must be launched on an Ariane 5. This spacecraft takes more than 9 years to reach the comet, arrives with a net spacecraft mass of 1300 kg, and is not

capable of returning a sample from the comet. The SEP-based CNSR spacecraft, on the other hand, has an initial-wet mass of 1830 kg and is launched on a Delta IV medium launch vehicle. The spacecraft takes only 2.6 years to reach the comet with a delivered mass of over 1300 kg and takes an additional 4.5 years to return a sample to Earth. Thus, the SEP-based CNSR spacecraft can travel to the comet and return to Earth in less time than it takes for the Rosetta spacecraft to fly to the comet!

Future deep-space missions will require multi-engine SEP systems, instead of the single-engine system used on DS1, with up to 4 engines operating at a time and processing up to 10 kW of power. In addition, these systems will require a significantly enhanced engine-throughput capability, operation at higher power levels per engine, and operation at higher specific impulses. The NSTAR service life assessment activity, which includes a combination of long-duration testing [5,6,16 to 18,25] and analyses [19 to 24] of the critical engine-wear-out-failure modes, indicates that the NSTAR engine can process a total propellant throughput of 130 kg with a low failure risk. Further analyses and extended testing of the DS1 flight-spare engine are planned to extend this throughput capability to larger values.

5.0 Acknowledgment

This publication was prepared at the Jet Propulsion Laboratory, California Institute of Technology, under a contract with the National Aeronautics and Space Administration.

6.0 List of References

[1] R. Kakuda, "NSTAR Flight Validation Report," MOR-602, JPL D-18219, internal document, November 1, 1999.

[2] J. S. Sovey, et al., "Development of an Ion Thruster and Power Processor for New Millennium's Deep Space 1 Mission," AIAA-97-2778, presented at the 33rd AIAA/ASME/SAE/ASEE Joint Propulsion Conference, Seattle, WA, June 1997.

[3] J. S. Sovey, V. K. Rawlin, and M. J. Patterson, "A Synopsis of Ion Propulsion Development Projects in the US: SERT I to DS1," AIAA-99-2270, presented at the 35th AIAA/ASME/SAE/ASEE Joint Propulsion Conference, Los Angeles, CA, June 1999.

[4] R. Kakuda et al., "NSTAR User Performance Needs Report," JPL D-12672, May 2, 1995.

[5] J. E. Polk, et al., "The Effect of Engine Wear on Performance in the NSTAR 8,000-Hour Ion Engine Endurance Test," AIAA-97-3387, presented at the 33rd AIAA/ASME/SAE/ASEE Joint Propulsion Conference, Seattle, WA, June 1997.

[6] J. E. Polk, et al., "An Overview of the Results from an 8,200-Hour Wear Test of the NSTAR Ion Thruster," AIAA-99-2446, presented at the 35th AIAA/ASME /SAE/ASEE Joint Propulsion Conference, Los Angeles, CA, June 1999.

[7] J. E. Polk, et al., "Validation of the NSTAR Ion Propulsion System on the Deep Space One Mission: Overview and Initial Results," AIAA-99-2274, presented at the 35th AIAA/ASME/SAE/ASEE Joint Propulsion Conference, Los Angeles, CA, June 1999.

[8] M. G. Marcucci and J. E. Polk, "NSTAR Xenon Ion Thruster on DS1: Ground and Flight Tests," I-18, presented at the 8th International Conference on Ion Sources, Kyoto, Japan, Sept. 6 to 10, 1999.

[9] G. B. Ganapathi and C. S. Engelbrecht, "Post Launch Performance Characterization of the Xenon Feed System on Deep Space One," AIAA-99-2273, presented at the 35th AIAA/ASME/SAE/ASEE Joint Propulsion Conference, Los Angeles, CA, June 1999.

[10] J. A. Christensen, et al., "The NSTAR Ion Propulsion Subsystem for DS1," AIAA-99-2972, presented at the 35th AIAA/ASME/SAE/ASEE Joint Propulsion Conference, Los Angeles, CA, June 1999.

[11] J. A. Hamley, et al., "The Design and Performance Characteristics of the NSTAR PPU and DCIU," AIAA-98-3938, presented at the 34th AIAA/ASME/ SAE/ASEE Joint Propulsion Conference, Cleveland, OH, July 1998.

[12] J. A. Christensen, et al., "Design and Fabrication of a Flight Model 2.3-kW Ion Thruster for the Deep Space 1 Mission," AIAA-98-3327, presented at the 34th AIAA/ASME/SAE/ASEE Joint Propulsion Conference, Cleveland, OH, July 1998.

[13] V. K. Rawlin, "NSTAR Flight Thruster Qualification Testing," AIAA-98-3936, presented at the 34th AIAA/ASME/SAE/ASEE Joint Propulsion Conference, Cleveland, OH, July 1998.

[14] J. J. Wang, et al., "Deep Space One Investigations of Ion Propulsion Plasma Interactions: Overview and Initial Results," AIAA-99-2971, presented at the 35th AIAA/ASME/SAE/ASEE Joint Propulsion Conference, Los Angeles, CA, June 1999.

[15] V. Rawlin, et al., "Thermal Environmental Testing of NSTAR Engineering Model Ion Thrusters," IEPC-97-051, presented at the 25th International Electric Propulsion Conference, Cleveland, OH, August 1997.

[16] J. E. Polk, et al., "Behavior of the Thrust Vector in the NSTAR Ion Thruster," AIAA-98-3940, presented at the 34th AIAA/ASME/SAE/ASEE Joint Propulsion Conference, Cleveland, OH, July 1998.

[17] M. J. Patterson, et al., "2.3-kW Ion Thruster Wear Test," AIAA-95-2516, presented at the 31st AIAA/ASME/SAE/ASEE Joint Propulsion Conference, San Diego, CA, July 1995.

[18] J. E. Polk, et al., "A 1,000-hr Wear Test of the NASA NSTAR Ion Thruster," AIAA-96-2717, presented at the 32nd AIAA/ASME/SAE/ASEE Joint Propulsion Conference, Lake Buena Vista, FL, July 1996.

[19] J. E. Polk, et al., "Probabilistic Analyses of Ion Engine Accelerator Grid Life," IEPC-93-176, presented at the 23rd International Electric Propulsion Conference, Seattle, WA, September 1993.

[20] J. E. Polk, et al., "Spatial and Temporal Distribution of Ion Engine Accelerator Grid Erosion," AIAA-95-2924, presented at the 31st AIAA/ASME/SAE/ASEE Joint Propulsion Conference, San Diego, CA, July 1995.

[21] J. R. Brophy, et al., "Ion Engine Service Life Validation by Analysis and Testing," AIAA-96-2715, presented at the 32nd AIAA/ASME/SAE/ASEE Joint Propulsion Conference, Lake Buena Vista, FL, July 1996.

[22] J. E. Polk, et al., "In Situ, Time-Resolved Accelerator Grid Erosion Measurement in the NSTAR 8,000-hr Ion Engine Wear Test," IEPC-97-047, presented at the 25th International Electric Propulsion Conference, Cleveland, OH, August 1997.

[23] J. R. Anderson, et al., "Service Life Assessment for Ion Engines," IEPC-97-049, presented at the 25th International Electric Propulsion Conference, Cleveland, OH, August 1997.

[24] J. R. Brophy, et al., "The Ion Propulsion System on NASA's Space Technology 4/Champollion Comet Rendezvous Mission," AIAA-99-2856, presented at the 35th AIAA/ASME/SAE/ASEE Joint Propulsion Conference, Los Angeles, CA, June 1999.

[25] J. R. Anderson, et al., "Results of an On-Going Long-Duration Ground Test of the DS1 Flight Spare Ion Engine," AIAA-99-2857, presented at the 35th AIAA/ASME/SAE/ASEE Joint Propulsion Conference, Los Angeles, CA, June 1999.

[26] J. A. Hamley, "NSTAR Thruster Element Technical Requirements Document," Technical Report D13638, Jet Propulsion Laboratory, Internal Document, 1997.

[27] M. J. Patterson, et al., "NASA 30-cm Ion Thruster Development Status," AIAA-94-2849, presented at the 30th AIAA/ASME/SAE/ASEE Joint Propulsion Conference, Indianapolis, IN, July 1994.

[28] K. D. Goodfellow, G. B. Ganapathi, and J. F. Stocky, "An Experimental and Theoretical Analysis of the Grid Clearing Capability of the NSTAR Ion Propulsion system," AIAA-99-2859, presented at the 35th AIAA/ASME/SAE/ASEE Joint Propulsion Conference, Los Angeles, CA, June 1999.

[29] W. R. Kerslake and L. R. Ignaczak, "SERT II 1980 Extended Flight Thruster Experiments," IEPC-81-665, presented at the 18th International Electric Propulsion Conference, Las Vegas, 1981.

[30] M. D. Rayman, et al., "Results from the Deep Space 1 Technology Validation Mission," IAA-99-11.2.01, presented at the 50th International Astronautical Congress, Amsterdam, The Netherlands, October 1999.

Appendix A. List of Telemetry Channels and Names

The IPS and spacecraft-data channels used for IPS diagnostics, trending analysis, and NSTAR archive storage are given in Table A1

Table A1. IGOR Data Channels

Channel	Title of Parameter	Channel	Title of Parameter	Channel	Title of Parameter
SCET		V0128	Shutdown Mode	V0198	PPU Status Word #2
ERT		V0129	Code Checksum	V0199	# of Recycles
V0001	EHA DCIU XIPS Mode	V0130	XFS Operating Mode	V0200	XFS Status Word
V0002	EHA PPU Status Word 1	V0131	Software Version #	V0201	Valve Status Word
V0003	EHA XFS Status Word	V0132	PPU Data Packet ID	V0202	# SV3 Cycles
V0004	EHA Mgr. Talking?	V0133	Accel Current	V0203	# SV4 Cycles
V0005	EHA Manager DCIU state	V0134	Accel Voltage	V0204	Continuous Dump Offset
V0006	EHA Last Command sent	V0135	Beam Current	V0205	Continuous Dump Segment
V0008	EHA DCIU state	V0136	Beam Voltage	V0206	Continuous Dump #0
V0009	EHA XIPS Mode	V0137	Discharge Current	V0207	Continuous Dump #1
V0010	EHA Thrust Mode	V0138	Dischrg Voltage	V0208	Continuous Dump #2
V0011	EHA Startup Mode	V0139	Discharge Heater Current	V0209	Continuous Dump #3
V0012	EHA Throttle Mode	V0140	Discharge Heater Voltage	V0210	Continuous Dump #4
V0013	EHA Accel Current	V0141	HV line current	V0211	Continuous Dump #5
V0014	EHA Beam Current	V0142	HV line voltage	V0212	Continuous Dump #6
V0015	EHA Beam Voltage	V0143	Neutralizer Current	V0213	Continuous Dump #7
V0016	EHA Discharge Current	V0144	Neu. Voltage	V0218	Continuous Dump #8
V0017	EHA Discharge Voltage	V0145	Neutralizer Heater Current	V0219	Continuous Dump #9
V0018	EHA Neutralizer Voltage	V0146	Neutralizer Heater Voltage	V0220	Peek Memory Offset
V0019	EHA Neutralizer Common	V0147	Neutralizer Common	V0221	Peek Memory Segment
V0020	EHA PT1 Pressure	V0148	+5V Ref	V0222	Peek Memory #0
V0021	EHA XFS Temperature TP1	V0149	PPU [RT-1] Temp	V0223	Peek Memory #1
V0022	EHA XFS Temperature TP4	V0150	PPU Temp. [RT-2, Neu. Sw., Q1]	V0224	Peek Memory #2
V0023	EHA Measured Press. 1	V0151	PPU Temp. #3 [RT-3, Screen]	V0225	Peek Memory #3
V0024	EHA Measured Press. 2	V0152	PPU Temp. #4 [RT-4, Disc. Rect.]	V0226	Peek Memory #4
V0025	EHA Echo DCIU command	V0153	+5V PPU	V0227	Peek Memory #5
V0026	# of IPS commands received	V0154	+15V PPU	V0228	Peek Memory #6
V0027	# of 1553 commands pending	V0155	–15V PPU	V0229	Peek Memory #7
V0028	Greatest # 1553 commands pending	V0156	Discharge Cmd Level	V2510	Gimbal Pot Voltage
V0029	IPS telemetry period	V0157	Discharge Heater Cmd Level	V2512	Gimbal 1 (+X+Y)
V0030	Lower mission power level	V0158	Neutralizer Cmd Level	V2520	Gimbal 2 Pot Voltage
V0031	Upper mission power level	V0159	Neutralizer Heater Cmd Level	V2522	Gimbal 2 (+X-Y)
V0032	DCIU thrust level	V0160	Screen Cmd Level	V3100	Boot Load Mode
V0033	Desired thrust duration (s)	V0161	Accelerator Cmd Level	V3101	Safe Mode Status
V0034	Thrusting?	V0162	PPU Digital Input: Bit 0 = Recycle Flag	V3102	Standby Mode
V0035	Thrust period cum.	V0163	PPU Digital Output	V3103	Grid Clear Mode
V0036	Cum. since last update	V0164	XFS Data Packet ID	V3104	Cathode Cond. Mode
V0037	Accumulated thrust mag.	V0165	PT1 Pressure	V3105	Thrust Mode
V0038	# of packets since last DCIU telem.	V0166	PA1 Pressure	V3106	XFS ON Mode

Channel	Title of Parameter	Channel	Title of Parameter	Channel	Title of Parameter
V0039	Processing recycle?	V0167	PA2 Pressure	V3107	XFS Initialization
V0040	DCIU heatbeat	V0168	PA3 Pressure	V3116	Recycle Flag
V0100	DCIU Data Packet ID	V0169	PA4 Pressure	V3132	Neutralizer Htr Enable
V0101	DCIU Time	V0170	PA5 Pressure	V3133	Discharge Htr Enable
V0103	DCIU command accepted counter.	V0171	PA6 Pressure	V3134	Neutralizer Enable
V0104	# Cmd rejected	V0172	XFS Temp TP1	V3135	Discharge Enable
V0105	Power Level Checksum	V0173	XFS Temp TP2	V3136	Beam Enable
V0106	Command #0	V0174	XFS Temp TP3	V3140	Thruster A Select
V0107	Command #1	V0175	XFS Temp TP4	V3141	Thruster B Select
V0108	Command #2	V0176	XFS Temp TP5	V3142	Grid Clear Enable
V0109	Command #3	V0177	XFS Temp TP6	V3143	Recycle Clear
V0110	Error #0	V0178	Main Flow Temp TJ1	V3148	Neutralizer Lit
V0111	Error #1	V0179	Cathode Flow Temp TJ2	V3149	Discharge Lit
V0112	Error #2	V0180	Neutralizer Flow Temp TJ3	V3150	Beam Supply Lit
V0113	Error #3	V0181	Regulator 1 Temp TR1	V3151	Grid Clear Required
V0114	# of Errors	V0182	Regulator 2 Temp TR2	V3152	Neutralizer Heater Open
V0115	DCIU +5V	V0183	SV1/3 Pulse Width	V3153	Discharge Heater Open
V0116	DCIU +15V	V0184	SV2/4 Pulse Width	V3154	Grid Clear Fail
V0117	DCIU -15V	V0185	SV1/2,3/4 Delay Width	V3156	Thruster A Status
V0118	+28V Bus Current	V0186	SV2/1,4/3 Delay Width	V3157	Thruster B Status
V0119	Processing Time	V0187	Latch Valve Width	V3158	Neutralizer Failed to Light
V0120	Power Level	V0188	Measured Pressure 1	V3159	Discharge Failed to Light
V0121	XIPS Mode	V0189	Required Pressure 1	V3160	Multiple Recycle Flag
V0122	Safe Mode	V0190	Measured Pressure 2	V3161	Continuous Recycle Flag
V0123	Grid Clear Mode	V0191	Required Pressure 2	V3162	Beam Control Enable
V0124	Cathode Conditioning Mode	V0192	Number SV1 Cycles	V3163	Diode Mode Enable
V0125	Thrust Mode	V0194	Number SV2 Cycles	V3164	Beam Voltage 5% error
V0126	Startup Mode	V0196	Status Data Packet	V3165	Beam Current 5% error
V0127	Throttle Mode	V0197	PPU Status Word 1	V3166	Accel Voltage 5% error
V3167	Accel Current 5% error	V3300	Shutdown Heaters Off	V4068	DSEU1 temp.
V3168	Discharge Voltage 5% error	V3301	XSHCLSVL	V4069	DSEU2 temp.
V3169	Discharge Current 5% error	V3319	XFS Initialization Mode	A0945	Pulses X3
V3170	Neutralizer Voltage 5% error	V3320	XFS Run Mode Status	A0947	Pulses X4
V3171	Neutralizer Current 5% error	V3329	Software Version - Minor Revision	A0949	Pulses Z1
V3172	Beam Voltage 10% error	V3330	Software Version - Major Revision	A0952	Pulses Z2
V3173	Beam Current 10% error	V3401	Ingested mass flow	A0954	Pulses Z3
V3174	Accel Voltage 10% error	V3402	Main flow rate	A0956	Pulses Z4
V3175	Accel Current 10% error	V3403	Cathode flow rate	A0958	Pulses X1
V3176	Discharge Voltage 10% error	V3404	Neutralizer flow rate	A0961	Pulses X2
V3177	Discharge Current 10% error	V3405	Total flow rate	A1401	Sun from X axis (Cos)
V3178	Neutralizer Voltage 10% error	V3406	Total main flow rate	A1402	Sun from Y axis (Cos)
V3179	Neutralizer Current 10% error	V3407	Total mass flow	A1403	Sun from Z axis (Cos)
V3180	XFS Normal Mode	V3408	Beam voltage	A1640	X3 RCS on-time
V3181	XFS Single Plenum Mode	V3409	Beam current	A1646	X4 RCS on-time
V3182	Single Main	V3410	Total Eng Pwr	A1650	Z1 RCS on-time
V3183	Single Cathode	V3411	Discharge loss	A1658	Z2 RCS on-time
V3184	Fault Protection Ena/Dis	V3412	Total prop. util. eff.	A1666	Z3 RCS on-time
V3185	XFS Initialized	V3413	Discharge prop. util. eff.	A1676	Z4 RCS on-time

Channel	Title of Parameter	Channel	Title of Parameter	Channel	Title of Parameter
V3196	Latch Valve #1 Open/Close	V3414	Xe double ion fraction	A1685	X1 RCS on-time
V3197	Latch Valve #2 Open/Close	V3415	Thrust loss factor	A1692	X2 RCS on-time
V3198	Latch Valve #3 Open/Close	V3416	Thrust	P2030	Solar Array Voltage
V3199	Latch Valve #4 Open/Close	V3417	Specific impulse	P2040	Solar Array 1 Current
V3200	Latch Valve #5 Open/Close	V3418	Overall thrust eff.	P2050	Solar Array 2 Current
V3201	Safe Mode Start	V3419	EHA mission power level	P2060	Essential Bus Current
V3202	Safe Mode Shutdown	V3420	EHA/IPS mission power level	P2061	Essential Bus Voltage
V3203	Safe Mode Close Valves	V3421	Mssn Th Chck Sum	P2062	Bus 1 Current
V3217	Grid Clear Start	V3422	P1 Measured - Req.	P2063	Bus 1S Current
V3218	Grid Clear Light Discharge	V3423	P2 Measured - Req.	P2064	Bus 2 Current
V3219	Grid Clear Check Jb	V3424	Vb Meas - Tbl	P2065	Bus 3 Current
V3220	Grid Clear Terminate	V3425	Vb Meas - Tbl	P3072	PPU Input Power
V3221	Grid Clear Reset	V3426	Va Meas - Tbl		
V3233	Cathode Conditioning Start	V3427	Ja Meas - Tbl		
V3234	Cathode Conditioning Heat 1	V3428	Vd Meas - Tbl		
V3235	Cathode Conditioning Cool 1	V3429	Jd Meas - Tbl		
V3236	Cathode Conditioning Heat 2	V3430	Vn Meas - Tbl		
V3237	Cathode Conditioning Cool 2	V3431	Jn Meas - Tbl		
V3238	Cathode Conditioning Terminate	V3435	Main Err. SV1 - SV2 Cycles		
V3239	Cathode Conditioning Reset	V3436	Cathode Err. SV3 - SV4 Cycles		
V3249	Thrust Startup	V3437	Set Beam Voltage		
V3250	Thrust Throttle	V3438	Set Beam Current		
V3251	Thrust Steady State	V3439	Set Accel Voltage		
V3252	Thrust Shutdown	V3440	Set Accel Current		
V3253	Thrust Shutdown XFS	V3441	Set Discharge Voltage		
V3265	Startup Start	V3442	Set Discharge Current		
V3266	Startup XFS Init	V3443	Set Neutralizer Voltage		
V3267	Startup Preheat Both	V3444	Set Neutralizer Current		
V3268	Startup Preheat Discharge	V3445	Set Main Pressure		
V3269	Startup Ignite Neutralizer	V3446	Set Cathode Pressure		
V3270	Startup Ignite Discharge	V3447	Set Single Plenum Pressure		
V3271	Startup Cool Both	V3448	Req. Cathode flow		
V3272	Startup Cool Discharge	V3449	Req. Neut. flow		
V3273	Startup High Voltage On	V3450	Main Flow Error		
V3274	Startup Ignition Failure	V3451	Main Cathode Error		
V3281	Throttle Start	V3452	Neutralizer Error		
V3282	Throttle Down Neutralizer	V3453	Req. Main flow		
V3283	Throttle Down Discharge	V4002	Temp		
V3284	Throttle Down Beam	V4051	DCIU Temp 1		
V3285	Throttle Down Accelerator	V4052	PPU Temp 1		
V3286	Throttle Down XFS	V4053	PPU Temperature 2		
V3287	Throttle Up Neutralizer	V4054	Xenon Temp		
V3288	Throttle Up Discharge	V4061	Gimbal 1 (+X+Y) Temp.		
V3289	Throttle Up Beam	V4062	Gimbal 2 Temp.		
V3290	Throttle Up Accelerator	V4063	Gim Brckt Temp		
V3291	Throttle Up XFS	V4064	Thrstr Msk Temp		
V3297	Shutdown Start (Beam Off)	V4065	Xe tank temp		
V3298	Shutdown Discharge Off	V4066	DCIU temp.		
V3299	Shutdown Neutralizer Off	V4067	Thruster Temp.		

Appendix B. Date of Turn-on/off and Frequency of Data Capture

DATE OF TURN-ON/OFF

Below is the list of the IPS technology validation activities and beam on and off times that took place on DS1. The total accumulated hours as of 1999-30T00:00 is 3575 hours. (Ken Fujii, 12/16/99.)

Table B1. Beam On/Off Time

Beam On Time	Beam Off Time	Duration (hr)	Event
1998-314T193426	1998-314T193926	0.08	Initial IAT Attempt
1998-328T225224	1998-342T220440	335.20	IAT0
1998-346T004902	1998-346T025300	2.07	IPS arc 1.1
1998-348T221838	1998-352T214040	95.37	IPS arc 1.1
1998-352T225317	1998-355T205537	70.04	IPS arc 1.1
1998-356T011959	1998-356T204419	19.41	IPS arc 1.1
1998-356T215719	1999-005T160009	330.05	IPS arc 1.1
1999-022T213604	1999-022T221636	0.68	SPeak
1999-057T231116	1999-058T001100	1.00	IPS Readiness Test
1999-075T071448	1999-081T195503	156.67	IPS arc 1.2 (C1A NBURN1)
1999-082T130932	1999-088T113958	142.51	IPS arc 1.2 (C1A NBURN2)
1999-089T040828	1999-095T160458	155.94	IPS arc 1.2 (C1A NBURN3)
1999-096T171034	1999-102T162959	143.32	IPS arc 1.2 (C1B NBURN1)
1999-103T090017	1999-109T162957	151.49	IPS arc 1.2 (C1B NBURN2)
1999-110T090642	1999-116T120458	146.97	IPS arc 1.2 (C1B NBURN3)
1999-117T042258	1999-117T173458	13.20	IPS arc 1.2 (C1B NBURN4)
1999-138T095155	1999-139T001015	14.31	RAX
1999-148T090818	1999-148T222257	13.24	IAT2
1999-165T160444	1999-165T201604	4.19	IPS Test TCM 1
1999-166T041229	1999-166T082604	4.23	IPS Test TCM 2
1999-204T225503	1999-205T011918	2.40	ACA-5 day TCM
1999-211T160802	1999-214T044617	60.64	Post Encounter NBURN
1999-214T220803	1999-221T065954	152.86	E1C NBURN
1999-222T042520	1999-228T075521	147.50	IPS arc 2.1 (C2A NBURN1)
1999-228T204023	1999-235T062023	153.67	IPS arc 2.1 (C2A NBURN2)
1999-237T025731	1999-242T211021	138.21	IPS arc 2.1 (C2A NBURN3)
1999-243T064953	1999-249T152033	152.51	IPS arc 2.1 (C2A NBURN4)
1999-250T025452	1999-256T174922	158.91	IPS arc 2.1 (C2B NBURN1)
1999-257T031431	1999-263T190922	159.91	IPS arc 2.1 (C2B NBURN2)
1999-264T085352	1999-270T183922	153.76	IPS arc 2.1 (C2B NBURN3)
1999-271T075502	1999-277T163922	152.74	IPS arc 2.1 (C2B NBURN4)
1999-278T054921	1999-284T162753	154.64	IPS arc 2.1 (C2C NBURN1)
1999-285T054831	1999-291T152752	153.66	IPS arc 2.1 (C2C NBURN2)
1999-292T061351	1999-293T114252	29.48	IPS arc 2.1 (C2C NBURN3)
1999-310T010846	1999-310T050757	3.99	MICAS Pointing Test

FREQUENCY OF DATA CAPTURE

The IPS telemetry rate was limited by the speed of spacecraft software, the size of the spacecraft memory, the spacecraft telemetry rate as a function of Earth distance, spacecraft orientation, the selected DSN station, and the needs of other competing users.

The maximum IPS data rate was 2048 bits per second. This occurred when all of the IPS data was sampled once every second. By selecting a smaller subset of data and sampling at a lower rate, the IPS data rate was varied from 2048 bits per second to 2 bits per second when the IPS was thrusting.

The limited speed of the spacecraft's telemetry system limited the maximum average IPS data-sample rate to once every two seconds (although one sample per second rate was used for short periods of time). Most of the early IPS telemetry was at a 10 seconds per sample rate, or 200 bits per second.

After initial IPS checkout, spacecraft telemetry was greatly reduced because of reduced link performance and DSN-station passes. The IPS-sample rate was reduced to one sample every 5 minute. This reduced the IPS data rate to less than 7 bits per second.

As the Earth distance increased, it was necessary to further reduce spacecraft telemetry. The IPS was sampled once every 15 minutes, resulting in a data rate of 2 bits per second. It is expected that the data rate will be reduced to 1/2 bit per second during the latter portion of the mission.

By using proper data selection, the data rate could be easily reduced by a factor of four. It is envisioned that, using onboard logic, future missions will not need to communicate with the IPS unless there is a fault.